Final Draft of the paper
https://ascelibrary.org/doi/10.1061/%28ASCE%29CF.1943-5509.0001049
published in the Journal of Performance of Constructed Facilities (ASCE)

Epistemic uncertainties in structural modeling: a blind benchmark for seismic assessment of slender masonry towers

Gianni Bartoli
Department of Civil and Environmental Engineering,
University of Florence
via di S. Marta 3 – I-50139 Florence – Italy
e-mail: gianni.bartoli@unifi.it

Michele Betti
Department of Civil and Environmental Engineering,
University of Florence
via di S. Marta 3 – I-50139 Florence – Italy
e-mail: mbetti@dicea.unifi.it

Paolo Biagini
Department of Civil and Environmental Engineering,
University of Florence
via di S. Marta 3 – I-50139 Florence – Italy
e-mail: pbiagini@gmail.com

Andrea Borghini
Department of Civil and Environmental Engineering,
University of Florence
via di S. Marta 3 – I-50139 Florence – Italy
e-mail: borghini@dicea.unifi.it

Alberto Ciavattone
Department of Civil and Environmental Engineering,
University of Florence

via di S. Marta 3 – I-50139 Florence – Italy
e-mail: alberto.ciavattone@dicea.unifi.it

Maria Girardi
Istituto di Scienza e Tecnologie dell'Informazione "A. Faedo", ISTI–CNR,
via G. Moruzzi 1, I-56124 Pisa – Italy
e-mail: Maria.Girardi@isti.cnr.it

Giovanni Lancioni
Department of Civil and Building Engineering, and Architecture,
Polytechnic University of Marche,
via Brecce Bianche 12, I-60131 Ancona – Italy
e-mail: g.lancioni@univpm.it

Antonino Maria Marra
Department of Civil and Environmental Engineering,
University of Florence
via di S. Marta 3 – I-50139 Florence – Italy
e-mail: antonino.marra@dicea.unifi.it

Barbara Ortolani
Department of Civil and Environmental Engineering,
University of Florence
via di S. Marta 3 – I-50139 Florence – Italy
e-mail: ortolani.barbara@gmail.com

Barbara Pintucchi
Department of Civil and Environmental Engineering,
University of Florence
via di S. Marta 3 – I-50139 Florence – Italy
e-mail: barbara.pintucchi@unifi.it

Luca Salvatori

Department of Civil and Environmental Engineering,
University of Florence
via di S. Marta 3 – I-50139 Florence – Italy
e-mail: luca.salvatori@unifi.it

ABSTRACT:

The paper reports the results of a blind benchmark developed as a part of the preliminary activity of the research project RiSEM (Italian acronym for Seismic Risk on Monumental Buildings). The benchmark was aimed at comparing the results obtained with different analytical models and/or numerical analysis techniques (variational approach, finite elements, macro-elements, equivalent frame, etc.) for the assessment of the nonlinear structural behavior of two cantilever masonry elements with different slenderness under increasing horizontal loads. The analyzed elements were characterized by a deliberately simple geometry, and the comparison between the numerical results had a twofold purpose. On the one hand, it aimed at estimating the effects of the epistemic uncertainties that are related to the different models and numerical techniques. On the other hand, it aimed at reaching a proper evaluation of the influence of parameters describing the post-elastic behavior of the structural typology analyzed within the research project (specifically, the masonry towers). Both these objectives were necessary to further proceed with the development of simplified numerical models needed for the subsequent risk analysis. For both slenderness, the results have highlighted a significant dispersion of both the displacement capacity and post-peak softening branch of the capacity curves. In addition, after some elaborations, it has been observed that the dispersion of the results is proportional to both the shear-force and displacement level.

KEYWORDS:

Epistemic uncertainties; Modeling techniques; Pushover analysis; Seismic assessment; Slender masonry towers; Unreinforced masonry.

Introduction

In the field of Civil Engineering, the use of proper mechanical models and numerical codes is frequently required to perform a broad range of tasks (*e.g.,* damage and/or structural identification, response predictions to various loads, etc.) whose results constitute an important support input for decision looking for structural problem solving. Usually solutions offered by the various modeling techniques are affected by a certain degree of uncertainty, which asks for a proper quantification by means of reliability analyses. Uncertainties affecting the physical systems can be grouped in two main categories: aleatory and epistemic uncertainties (Helton and Oberkampf 2004). The first group collects the uncertainties that are typically due to the randomness of the natural phenomena; these uncertainties are unavoidable but today they can be efficiently approached within the framework of probability theory (Lin 1967, Lin and Cai 1995). The second group considers the inaccuracy due to the lack-of-knowledge. Several sources of inaccuracy can occur and, generally, epistemic uncertainties collect a wide range of potential incomplete knowledge: the hypotheses underlying a model (*i.e.* the ability of the model to describe the system of interest, together with the model simplifications), the uncertainty in the model parameters, the observation errors, the uncertainty on the software development, etc. (Der Kiureghian and Ditlevsen 2009).
While aleatory uncertainties are typically irreducible and non-subjective (since they are intrinsic with the variations associated to the physical environment under consideration and/or with uncertainties in resistance and other parameters of structural materials), the epistemic uncertainties are (potentially) reducible since they are substantially due to ignorance or roughness in modeling the overall physical environment. In last decades the distinction between aleatory and epistemic uncertainties has become very significant. According to Pan et al. (2011), the factors that may contribute to originate epistemic uncertainties can be classified as follows: 1) Vagueness (information that is imprecisely defined, unclear, or indistinct); 2) Non specificity (presence of several plausible alternatives); 3) Dissonance (existence of totally or partially conflicting evidence); 4) Ignorance. A general discussion on the classification of epistemic uncertainties is reported in Der Kiureghian and Ditlevsen (2009), where the interested reader is referred.
The increasing interest of the scientific community toward the systematization of this class of uncertainties, and their treatment, is demonstrated by the growing number of researches (Most 2011; Bradley 2010; Lagomarsino 2011; Tondelli et al. 2012) that spread the concept of epistemic uncertainties in those fields of engineering where the effects of the lack-of-knowledge were (but still are) traditionally assessed by heuristic sensitivity approaches. In Earthquake Engineering, the sources of uncertainty due to the earthquakes characteristics (intensity and record-to-record

variability) are commonly classified as aleatory uncertainties; while the uncertainties on mechanical parameters, constitutive models and cyclic behaviors are related to epistemic uncertainties.

Among all the potential sources of epistemic uncertainties, the paper aims to deepen the effects of the so-called model framework uncertainties, *i.e.* those uncertainties that are due to the uncertainty in the underlying science and algorithms of a numerical model or an analytical approach. This class of epistemic uncertainty is fairly broad, and includes several sources of vagueness/ignorance (Der Kiureghian and Ditlevsen 2009); among them: incomplete scientific data; lack-of-knowledge about the factors that control the behavior of the system being modeled; the effects of the hypotheses affecting the mechanical models; the effects deriving from the use of a model outside the framework for which it was originally developed. This is, in fact, an actual challenge for the scientific community since, with the advance of technology, modeling and simulation are increasingly used in engineering science, and their complexity is correspondingly growing in order to treat more sophisticated nonlinear physical processes. Nevertheless, more sophisticate modeling requires more input variables to characterize the physical problem, this leading to additional greater (epistemic) uncertainties. In addition, numerical models are usually tuned through comparison with available experimental results (the models are fitted in order to reproduce a reduced number of measurements identifying the unknown input parameters by an inverse strategy) but, at the same time, they are employed to predict the structural behavior under exceptional loads, and predictions for new extreme load cases may be inaccurate. This is true in general, but in case of the modeling of masonry constructions the problem is amplified by the great, and growing, number of approaches and numerical models proposed by the research community (Theodossopoulos and Sinha 2013).

Discussion of these uncertainties, and their effects, is herein approached through the results of a blind benchmark on the seismic assessment of cantilever masonry beams. The benchmark was developed within one of the research lines of the project “RiSEM - *Rischio Sismico negli Edifici Monumentali*” (Seismic Risk on Monumental Buildings), a research project funded by the Tuscany Regional Administration (Italy) that lasted from 2011 to 2013. The project aimed, through the creation of a network gathering complementary expertise, at deepening the technical and scientific knowledge in the field of the seismic assessment of monumental masonry buildings, with specific reference to historic masonry towers. Taking into account the difficulties that arise in developing exhaustive experimental campaigns in monumental building by traditional techniques, the project aimed at developing expeditious methodologies to evaluate the main structural characteristics needed for the subsequent seismic assessment at territorial scale.

The blind benchmark was focused at assessing the effects of model framework uncertainties on those parameters that are of primarily relevance for the definition of the seismic vulnerability of this typology of structures (herein idealized as a cantilever beam). The benchmark compared the results offered by different analytical models and numerical analysis techniques (variational approach, finite elements, macro-elements, equivalent frame, etc.) in the definition of the structural behavior under horizontal loads of two cantilever masonry elements characterized by different slenderness. The comparison between the results obtained by different models and computer codes has a twofold purpose. On the one hand, the estimation of the effects of the epistemic uncertainties (which are herein mainly related to the different analytical models and numerical analysis techniques adopted); on the other hand, the definitions of the parameters which describe the crisis of the structural elements (in order to further proceed with the development of simplified numerical models). The aim, therefore, is not to calibrate the mechanical and numerical parameters in order to reproduce experimental or reference results, but to evaluate (assuming a minimum common set of material parameters) the potential errors made in the prediction of the nonlinear behavior of a simple structural system using different numerical and/or analytical approaches.

The paper is organized as follows: in a first section the blind benchmark is described together with the employed mechanical parameters, while the numerical models are briefly described in a subsequent section. After, the results are summarized and critically compared; some conclusions are reported at the end of the paper.

Description of the blind benchmark

The idea was to perform a blind benchmark among several research groups working in the field of numerical modeling of the nonlinear structural behavior of masonry structures. Each researcher has chosen the proper modeling technique, based on his own experience. The benchmark is a “blind” one as no reference with existing data is done: “real” results are not known and they will never be available, so every researcher has to do his/her best to guess which were the ultimate capacity of a given structural elements without any proof of what he/she is assessing is correct. The same reliability level has been given to each of the analyses, even if an “expert a priori judgment” could have been assessed to those methods and analyses which are known not to be as accurate as others in facing the proposed problem.

Geometric characteristics and mechanical properties

The request of the benchmark was the one of determining the ultimate load and displacement under an increasing horizontal load of two simple cantilever masonry panels (Figure 1), characterized by different slenderness. The first case study, in particular, was a purely theoretical panel with dimensions 10 (B, width) × 40 (H, height) × 1 (t, thickness) meters; dimensions in the second case were given as follows: 4 × 40 × 1 ($B \times H \times t$) meters. The two cantilever beams will be respectively referred to as [10 × 40] and [4 × 40] in the following. Both panels are forced to undergo a plane stress or strain state, that is they are mainly compressed and bent normally to their thickness. The slendernesses of the case studies, $\lambda=H/B=4$ for the first case and $\lambda=10$ for the second one, were selected in order to cover a wide enough range of slenderness of existing masonry tower according to the goals of the research project RiSEM. Such slenderness may range, taking into account Italian historic towers, between 3 (Pighin tower in Rovigo; Valente and Milani 2016) and 10 (Mangia tower in Siena; Pieraccini et al. 2014). The differences in slenderness, moreover, allow analyzing different failure modes (for bending or shear). Both panels were assumed fixed at the base.

The mechanical properties adopted in the models were assumed on the basis of some experimental results obtained through in-situ shear-compression tests on a historic masonry (Galano and Vignoli 2001; Chiostrini et al. 2003) characterized by a chaotic texture made of stone or mixed stones and bricks masonry; the thickness of the panels varied from about 300 mm to about 600 mm (Chiostrini et al. 2003). Elastic parameters are reported in Table 1, together with the compressive and tensile strength. The weight of the masonry was assumed equal to 18 kN/m^3. Even if a suggested value for Poisson's coefficient was reported as an input of the benchmark, in several models a null value was used. The same was for the tensile and shear strength, assumed null in some models. Additional physical parameters, when required by each modeling approach, are specified in the corresponding section; they have been chosen and used independently by all the authors in their numerical modeling.

The performed analysis

To model the seismic capacity of the panels, nonlinear static analyses with uniform load distributions, monotonically increased up to failure, were performed. This procedure, now common in the structural engineering practice, is used to obtain an estimation of the so-called capacity curve of a structure (to be compared with the seismic demand), which represents a basic datum to predict both strength and ductility of the structure under consideration. With the aim to compare the different approaches, the capacity curves were evaluated, and the comparison was performed by taking directly into account the pushover curves calculated by each code in term of dimensionless shear, $\alpha = V/W$, being V the base shear and W the total weight of the beam. The ratio at the base of the cantilever beam is hence plotted against the ratio between the horizontal displacement d of the center of mass of the upper section of the beam and the beam height, H, that is by considering as a displacement parameter the drift $\theta = d/H$ (Figure 1).

Numerical models and analytical approaches

The blind benchmark aims at quantifying the effects of the epistemic uncertainties associated with the different modeling approaches (model framework uncertainties). To this end, the benchmark tests consider a wide class of analytical models and numerical analysis techniques. A first class of models includes numerical approaches specifically implemented to analyze the seismic response of masonry buildings (3Muri, 3DMacro), and resorts in different level of assumptions and simplification. A second class of numerical applications includes some general-purpose finite element (FE) codes, distributed under both commercial (DIANA, ANSYS) and OpenSource (Code ASTER) licenses. Each code adopts a different approach to model the nonlinear behavior of masonry. An additional class of research numerical instruments has been moreover tested (NOSA-ITACA, MADY, SMARTmasonry, VDM), specifically designed and developed within the Authors' research groups to model the mechanical behavior of masonry constructions. Although the selected codes were chosen with the aim to cover a wide and representative range of tools commonly employed (or that can be employed) to reproduce the specific nonlinear behavior of masonry and masonry structures, additional approaches are today available. Among them, it is noteworthy, f.i., the combined finite discrete element method (FDEM) (Munjiza 2004). In addition, with specific reference to the general purposes FE codes, worth noting are also, even if not employed in this research, the codes ABAQUS (Tarque et al. 2014), ADINA (Bennati et al. 2005) and LUSAS (Adam et al. 2010). To report an exhaustive review is almost impossible, and the interested reader is referred to Theodossopoulos and Sinha 2013 and Asteris et al. 2015.
Depending on the considered numerical approach, the problem has been analyzed by using one or two-dimensional elements (with the assumption of plane stress or strain problem, depending on the model framework), in other cases by using three-dimensional brick elements, depending on the characteristics of the specific code. An overview of such numerical methods, as well as a brief description of their specific theoretical aspects, is provided in order to allow easy comparison.

3Muri

The software 3Muri is a user-friendly computer code specifically proposed for the seismic analysis of regular masonry buildings through pushover analyses. The code, originally developed at the University of Genoa (Italy) and subsequently implemented in the commercial software 3Muri (Cattari et al. 2004; Lagomarsino et al. 2013), uses an equivalent frame modeling (EFM) approach according which the structure is idealized as a combination of one-dimensional macro-elements and is analyzed as a framed structure. Therefore, each wall of the masonry structure is subdivided into piers and spandrels, modeled with the one-dimensional macro-elements, which are connected by rigid nodes. The in-plane behavior of the macro-elements, both piers and spandrels, is assumed as elastic-perfectly plastic, with shear resistance and ultimate displacement obtained according the provisions of the Italian Code (NTC2008, 2008). In particular, the ultimate shear resistance is evaluated as the minimum between the resistance values for bending and diagonal cracking (in case of existing structures); while the ultimate displacement is conventionally assumed as a percentage of the height of the macro-element, considering the corresponding typology of collapse. The software, being based on the EFM approach, needs a limited number of degrees of freedom (DOFs) and it is hence possible to analyze large regular masonry structures with a reduced computational effort. Herein some attempts were done in order to employ the code to analyze a cantilever masonry beam. The application is hence interesting in order to evaluate the effects deriving from the use of a model outside the framework for which it was originally developed.

The [10 × 40] cantilever beam as a first attempt was discretized by using only one macro-element (Figure 2a). Due to the fact that the distribution of the horizontal load is composed of a single force on the top of the macro-element, this discretization does not allow the reproduction of the uniform load distribution. In order to obtain a uniform load distribution, a sensitivity analysis was hence performed dividing the structure into several horizontal levels, starting from the initial single macro-element (1×1) until 12 macro-elements (1×12) (Figure 2a - d). The pushover curves show a convergence on both the collapse multiplier and the drift obtained with a 12 macro-elements discretization, which allowed the reproduction of the uniform horizontal load distribution: the collapse multiplier α converges to the value of 0.20, while the maximum drift θ is approximately equal to 4‰. Starting from the (1×12) discretization, a subsequent sensitivity analysis was carried out in order to assess the influence of the slenderness of each macro-element, dividing them along the base length. In the starting discretization (1×12 configuration), the macro-element dimensions are 10.00 × 3.33 m, with slenderness h_e/b_e=0.33 (being h_e the height of the elements and b_e their base). From this configuration, 2×12 (Figure 2e), 3×12 and 4×12 (Figure 2f) configurations were analyzed. In the last configuration the size of each macro-element was 2.50 × 3.33 m, with a slenderness h_e/b_e=1.33. The comparison of the pushover curves showed that both the collapse multiplier and the initial stiffness (up to about the 60% of the maximum multiplier) are the same in each discretization. On the contrary, a dispersion was observed with respect to the ultimate drift, with a stabilization around the value of 8‰ with the model (4×12). This model was hence assumed as representative of the cantilever beam: it provides a collapse multiplier equal to 0.193 and a maximum displacement equal to 8.3‰ of the total height (Table 5). The first elements that collapse are the ones at the ground level where the axial load decreases during the evolution of the analysis, reducing the shear strength of the considered elements.

With respect to the [4 × 40] cantilever beam, as in the previous case, the division into 12 levels along the height showed a convergence of the collapse multiplier to the value of 0.075, while the maximum drift is approximately 9.5 ‰. Starting from this discretization (1×12 configuration), the influence of the slenderness of the macro-elements on the behavior of the beam was again investigated. In the first model (1×12 configuration) the dimensions of macro-element were 4.00×3.33 m, with slenderness h_e/b_e=0.83. Subsequently, 2×12, 3×12 and 4×12 configurations were evaluated. In the last configuration the size of each macro-element was 1.00 × 3.33 m, with a slenderness h_e/b_e=3.33. As in the previous case both the collapse multiplier and the initial stiffness are the same in each discretization. The ultimate drift ranges from a value of 9.5‰ (1×12) up to a value equal to 15.1‰ (2×12, 3×12, 4×12). In this case, the representative model was the one with the 2×12 macro-elements discretization, where the elements dimension is 2.00×3.33 m with slenderness equal to 1.67 (similar to the one of the beam [10 × 40]). The representative (2×12) model provides a collapse multiplier equal to 0.076 and a maximum displacement equal to 15.1‰ of the total height. Even in this case, the collapse occurs due to the excessive bending at the base: the vertical load became low with respect to compressive strength, the horizontal loads originate tensile flexural cracking at left corner, and the panel begins to behave as a nearly rigid body rotating around the toe with rocking.

3DMacro

The code 3DMacro, originally developed at the University of Catania (Italy) and subsequently implemented in the commercial software 3DMacro, allows the analysis of the seismic behavior of masonry buildings by using a two-dimensional macro-elements approach (Caliò et al. 2005). The macro-element, in its first version, was a plane pinned quadrilateral element built with four rigid edges. Two diagonal springs connect two opposite corners to simulate the masonry wall shear behavior. Additional discrete distributions of nonlinear springs, with limited tension strength, are employed to connect the rigid edges of neighboring macro-elements to simulate its interaction. Springs normal to the sides of the macro-elements are introduced to simulate the axial and bending deformability and to account for the crushing and flexural collapses, while parallel springs simulate the sliding along macro-elements. The whole set of springs allows to properly simulate the nonlinear in-plane behavior of masonry buildings through the effective reproduction of the main in-plane collapse mechanisms of the masonry (flexural, shear-diagonal and shear-sliding failure). To account for the out-of-plane collapse behavior of masonry walls the plane macro-element was recently enriched by introducing a third dimension with additional nonlinear springs and additional DOFs (Caliò et al. 2008; Caliò et al. 2012). Both the plane two-dimensional macro-element and the enriched three-dimensional one allow a discrete equivalent representation of a masonry structure by assembling the macro-elements: a masonry panel, considering its dimensions, can be modeled with a unique macro-element or with a mesh of elements. Because of the reduced number of DOFs (in case of meshing with two-dimensional macro-element, each panels has 4 DOFs) the approach requires a suitable computational demand. Furthermore, only few parameters are required to characterize the nonlinear behavior of the masonry material: the elastic E_w and shear G_w modulus, the masonry compressive strength f_{wc} and the characteristic shear strength of the masonry τ_k. Additional parameters required by the code are the distance between the interface nonlinear springs and their ductility (both in tension and compression). Through the code, the seismic behavior of a masonry building is evaluated by performing pushover analyses.

As a first step, in order to reproduce the uniform distribution of the lateral load, a discretization along the height of the cantilever beams was performed. A parametric analysis was conducted by varying the height of the macro-elements and additional analyses were performed to investigate the influence of the horizontal dimension of the macro-elements and of the parameters defining its behavior (such as the distance between the interface springs). It was verified that the analyzed results, such as the collapse multiplier of the lateral load as well as the ultimate horizontal drift, are not significantly influenced by the variations of the investigated parameters (*i.e.* both the pushover curve and the collapse mechanism do not change). As a final mesh, the discretization of cantilever beam in macro-elements involves the use of 16 macro-elements (dimensions 5×5 m) for the [10 × 40] cantilever beam (Figure 3c) and 8 macro-elements (dimensions 4×5 m) for the [4×40] cantilever beam. As a second step, several parametric analyses were performed to assess the stability of the results with respect to the spacing between the interface nonlinear springs and their ductility. After the test, in both cases, the distance between the interface nonlinear springs was assumed equal to 25 cm (*i.e.* about 20 spring each side). Suggested default values were maintained for the spring ductility. The model of the cantilever beam [10 × 40] provides a collapse multiplier equal to 0.212 and an ultimate drift equal to about 4 ‰ (Table 5). For the model of the cantilever beam [4 × 40] the collapse multiplier is about 0.076 and the ultimate drift about 10‰ (Table 6). In both cases, the collapse occurs due to a flexural mechanism at the basement; both panels develop tensile cracks in the interfaces. Figure 3 shows the collapse mechanism for the beam [10 × 40].

DIANA

The commercial FE code DIANA was used to model the two slender cantilever masonry beams using three-dimensional (3D) 6-node isoparametric wedge elements (*TP18L,* Figure 4a). These elements were selected to avoid mesh dependence of the cracks. After meshing, the final 3D numerical model of the first cantilever beam [10 × 40] (Figure 4b) consisted of 1,804 nodes, 2,400 3D *TP18L* elements, corresponding to 5,280 DOFs. The final 3D numerical model of the second cantilever beam [4 × 40] consisted of 820 nodes, 960 3D *TP18L* elements, for a total of 2,400 DOFs. Displacements of the base nodes were fixed and, in addition, displacements of nodes in the transversal direction were also set equal to zero to analyze the plane strain state problem.

In order to model the cracking/crushing behavior, two models based on total strain (stress is defined as a function of strain) are implemented in DIANA. The first model is the Total Strain Crack Rotating (TSCR) where the stress-strain relationship is evaluated in the principle direction of the strain vector. The second one is the Total Strain Crack Fixed (TSCF), where the stress-strain relationship is evaluated in a fixed coordinate system which does not change once cracking is initiated. Both models are smeared-crack models according to which the localized cracking phenomenon is simulated in a disseminated way (taking advantage of the mesh-assembly of the FE model in order to facilitate numeric computation) and both models allow the possibility of forming two orthogonal cracks in each integration point. In this study the TSCF was employed since it has been shown that this model is more appropriate for most engineering purposes (Lourenço et al. 1998). The compressive uniaxial behavior is characterized by a linear stress-strain relation until about one third of the compressive strength, followed by a parabolic relation for the hardening regime until reaching the compressive strength and another parabolic branch for the post-peak softening according the Thorenfeldt model (Thorenfeldt et al. 1987). This model was chosen since its formulation does not depend on the fracture energy and only the compressive strength and the Young's modulus are required. The tensile uniaxial behavior is modeled according the linear tension softening model of Hordijk with exponential softening behavior in tension (Hordijk, 1991) assuming a constant shear retention factor *ß*. This factor accounts for the residual strength (or friction) between the two surfaces of a crack.

The values of the inelastic parameters required by the models were selected to reproduce the uniaxial compressive and tensile strengths reported in Table 1, and are summarized in Table 2.

The fracture energy (corresponding to the integral of the stress-displacement diagram for uniaxial stress and equating the energy needed to create a unit area of a fully developed crack) was estimated by:

$$G_f = \frac{f_{wt}^2 \cdot h}{0.739 \cdot E_w} = 38.97\ N/m \tag{1}$$

where $h = \sqrt[3]{V} = 0.75\,m$ denotes the crack bandwidth and *V* is the volume of the element. It is noteworthy that, using a smeared-crack model, the fracture energy must be normalized according to an equivalent length *h* in order to obtain mesh-objective results with respect to the mesh refinement. The crack bandwidth *h* depends on the elements type, size, shape, integration scheme, etc. For the models employed within this study, DIANA assumes the default crack bandwidth *h* to be the cubic root of the volume (all of the elements are solid elements).

The model of the cantilever beam [10 × 40] provides a collapse multiplier equal to 0.195 and an ultimate drift equal to about 8 ‰ (Table 5). For the model of the cantilever beam [4 × 40] the collapse multiplier is about 0.084 and the ultimate drift about 22.5‰ (Table 6). The cracking pattern and vertical stresses corresponding to the maximum base shear obtained with the [10 × 40] cantilever masonry beam are reported in Figure 4c.

Code ASTER

The two slender cantilever masonry beams were also modeled by means of Code ASTER (acronym of "Analyses des Structures et Thermo-mécanique pour des Études et des Recherches"), an Open Source FE solver employed for numerical simulations of materials and structures developed at the department "Analyses Mécaniques et Acoustiques" of Électricité de France (EDF). The implementation of the code began in 1989, to meet the internal needs of EDF in the nuclear industry, and it was released under the terms of the GNU GPL license in 2001. Under the Linux operative system, Code ASTER is directly integrated with the platform Salome-Meca (a multi-purpose platform for Pre- and Post-Processing for numerical simulation). The validation of the code was extremely careful, many comparisons with experimental results and benchmarks with other codes have been carried out by independent bodies by EDF. The code is particularly robust, containing about 1,500,000 lines of code (written both in Fortran and in Python).

Through the code the two cantilever beams were modeled by using three-dimensional (3D) 8-node isoparametric elements and, after meshing, the final 3D numerical model of the first cantilever beam [10 × 40] (Figure 5a) consisted of 11,907 nodes, 9,600 3D elements, totalling 23,400 DOFs. The final 3D numerical model of the second cantilever beam [4 × 40] (Figure 5b) consisted of 6,237 nodes, 4,800 3D elements, corresponding to about 12,250 DOFs. Displacements of the base nodes were fixed, and displacements of nodes in the transversal direction were zeroed to account for a plane strain state problem.

The concrete damage model of Mazars (Mazars and Pijaudier-Cabot 1989) was employed to model the masonry nonlinear behavior. The model refers to the continuum damage mechanics, according to the progressive degradation of material stiffness, due to the propagation of micro-cracks, is described through a continuous approach. The damage model of Mazars is an isotropic scalar damage model that assumes the damaged stiffness tensor as a scalar multiple of the initial elastic stiffness tensor. The damage is characterized by a single scalar variable, the damage index, ranging between 0 (no damage) and 1 (complete loss of strength). Due to the assumption of isotropic behavior, the stiffness degradation in different directions decrease proportionally and is independent of the loading direction. In addition, being a single scalar damage index model, it assumes that the Poisson's ratio is not affected by damage (the relative reduction of all the stiffness coefficients is the same). Strictly speaking, isotropic Mazars constitutive model could not be satisfactory when used for modeling masonry structures, where orthotropic or anisotropic modeling should be used. Nevertheless, it has to be observed that in many practical applications this approach is normally retained as acceptable despite the level of approximation.

Mazars damage evolution law is expressed in an explicit form, relating damage parameter and scalar measure of largest reached strain level in material, taking into account the principle of preserving of fracture energy G_f**.** The model of Mazars is implemented in the code in two versions. The first is a local approach where the stress at a point depends only on the deformation in the same point. The second is a nonlocal version where local stresses depend not only on the deformation of that point, but on the average strain defined in the neighborhood of the point. In this study the local version was employed, being less computational demanding. Hence a preliminary sensitivity analysis on the mesh size was performed to avoid stagnation of the results toward non-physical solution (*i.e.* objectivity of the results with respect to the finite element mesh was investigated).

Apart the two elastic parameters (the Young's modulus and the Poisson's coefficient) the definition of the model of Mazars requires 6 additional parameters, as reported in Table 3. The values of the parameters were selected reproducing a uniaxial test on a cube with a material with the compression and tension strength reported in Table 1. It is worth noting that, with this model, cracks at a microscopic point have no particular direction and a macroscopic crack is then defined as the locus of damage points. In fact, one of the advantages of such a model is the independence of the analysis with respect to cracking directions, which can be simply identified a posteriori once the nonlinear solution is obtained.

The damage map at collapse is reported (both for the [10 × 40] and the [4 × 40] cantilever masonry beams) in Figure 5, while the principal compressive stresses are reported in Figure 6.

ANSYS

The commercial FE code ANSYS was used to model the two masonry beams by means of three-dimensional 8-nodes isoparametric finite elements. The classical smeared-crack approach was employed and the mechanical nonlinear behavior of masonry was modeled via two approaches.

In a first case the Willam-Warnke (WW) failure criterion was employed (Willam and Warnke 1975). This failure criterion, initially adopted for concrete, accounts for both cracking and crushing failure modes through a smeared model. Despite the needing for five constants to define the criterion, in most practical cases (thereby when the hydrostatic stress is limited by $\sqrt{3}\, f_c$) the adopted failure surface is specified by means of only two constants: F_t and F_c (the uniaxial tensile and compressive strength respectively). A shear transfer coefficient β is introduced (depending on the crack status: open - β_t - or re-closed - β_c -) to take into account a shear strength reduction factor for those subsequent loads inducing sliding (shear) across the crack face.

In a second case the Willam-Warnke failure criterion was combined with the Drucker-Prager plasticity criterion (DP) originally proposed for geo-materials (Drucker and Prager 1952). In this case, as a result, the material behaves as an isotropic medium with plastic deformation, cracking and crushing capabilities. The material parameters required to define the model, the cohesion c and the internal angle of friction φ, are introduced in such a way that the circular cone yield surface of the DP model corresponds to the outer vertex of the hexagonal Mohr-Coulomb yield surface. The constitutive parameters used for the DP criterion and the WW failure domain are reported in Table 4 (Model 1 combines the WW failure criterion with the DP plasticity one, while Model 2 adopts the WW failure criterion alone). It is noteworthy to highlight the difference of the tensile and compressive strengths of the DP criterion (f_{tDP} = 0.34 N/mm^2, f_{cDP} = 5 N/mm^2) and those of the WW failure criterion (F_t = 0.24 N/mm^2, F_c = 6.0 N/mm^2). The combination of these parameters allows for an elastic-brittle behavior in case of biaxial tensile stresses or biaxial tensile-compressive stresses with low compression level. On the contrary, the material is elastoplastic in case of biaxial compressive stresses or biaxial tensile-compressive stresses with high compression level (Betti et al. 2016).

The load control Newton-Raphson method was selected to solve the nonlinear equations and the analyses were carried out by assuming a plane strain state; the Poisson's coefficient was assumed equal to zero. Analyses were eventually conducted with and without geometric non linearities. Preliminary tests were conducted to estimate the optimal mesh size, and the adopted size was 0.5×0.5×0.5 m. Consequently, after meshing, the final 3D numerical model of the first cantilever beam [10 × 40] consisted of 5,103 nodes, 401 3D *Solid65* elements, corresponding to 15,120 DOFs. The final 3D numerical model of the second cantilever beam [4 × 40] consisted of 2,187 nodes, 1,280 3D *Solid65* elements, for a total of 6,470 DOFs. Increasing the number of finite elements did not lead to any variation of results.

The cracking pattern obtained at collapse is reported, both for the [10 × 40] and the [4 × 40] cantilever masonry beam in Figure 7, while the principal compressive stresses are reported in Figure 8.

NOSA – ITACA

The FE code NOSA (acronym of “NOn-Linear Structural Analysis”) has been developing since the 1980s, by the Mechanics of Materials and Structures Laboratory of ISTI – CNR in Pisa, Italy (Lucchesi et al. 2008), with the aim of testing new constitutive models for material. Within the code, masonry is modeled as a homogeneous nonlinear elastic material with zero tensile strength and either infinite or finite compressive strength (Del Piero 1989; Di Pasquale 1992) according to the framework of no-tension (masonry-like) materials. The NOSA code has been successfully applied to the static analysis of several historical masonry buildings (Lucchesi et al. 2008; Girardi et al. 2015) and more recently to the seismic and dynamic analysis of masonry towers, beams and domes (Binante et al. 2012).

The constitutive model and numerical techniques for solving equilibrium problems of masonry constructions implemented in NOSA are described in Lucchesi et al. (2008). Briefly, masonry is modeled as a nonlinear hyperelastic material with Young's modulus, E>0, Poisson ratio ν (where $0 < \nu < 1/2$), zero tensile strength and maximum compressive stress $\sigma_0 < 0$. *Sym* indicates the vector space of symmetric tensors, while Sym^- and Sym^+ stand for the subsets of *Sym* constituted by the negative and positive semidefinite tensors, respectively. It is assumed that the infinitesimal strain, $\mathbf{E} \in Sym$, is the sum of an elastic part, $\mathbf{E}^e \in Sym$, and two mutually orthogonal inelastic parts, $\mathbf{E}^f \in Sym^+$ and $\mathbf{E}^c \in Sym^-$, respectively called fracture strain and crushing strain. It is moreover assumed that the Cauchy stress **T** depends linearly and isotropically on $\mathbf{E}^e$. Finally, some orthogonality conditions are imposed among tensors, to describe the elastic behavior of the material, which cracks and crushes without dissipating energy. By exploiting the coaxiality of **E**, **T**, $\mathbf{E}^f$ and $\mathbf{E}^c$, the stress tensor **T** satisfying the constitutive equation can be expressed as a nonlinear function of the total strain **E**. The explicit expression for **T(E)** can be found in Lucchesi et al. (2008), together with its derivative with respect to **E**. These expressions are then implemented in the Newton-Raphson scheme for solving the nonlinear algebraic system derived from discretisation of the equilibrium problem.

In recent years NOSA code has been further enhanced within the framework of the NOSA – ITACA project (www.nosaitaca.it/en) by integrating the NOSA code with the Open Source platform Salome-Meca (employed to provide the pre-post processing environments for defining geometries and visualizing results). The NOSA code has been substantially modified and equipped with new finite elements, thus extending its application capabilities. An efficient implementation of numerical methods for constrained eigenvalue problems, which enables conducting modal structural analyses while taking into account the features of master-slave constraints (tying or multipoint constraints), has been also embedded in NOSA (Porcelli et al. 2015).

The two slender masonry structures in the benchmark test have both been modeled via the NOSA – ITACA code using eight-node plane stress elements. The assumed mechanical properties are those reported in Table 1, except for the uniaxial tensile strength f_{wt}, which has set equal to zero. For the beam [4 × 40], a mesh composed of 640 elements has been used, while 1600 elements were used to discretize the [10 × 40] beam. After the dead load has been applied, the uniform lateral load is subsequently increased incrementally and the nonlinear equilibrium equations are solved by means of the Newton-Raphson scheme. It has been shown in Lucchesi et al. (2008) that the solution to the equilibrium problem of masonry-like materials is unique in terms of stress, while special attention is required when computing the displacements field. The results of the present pushover analyses have been carefully tested for different meshes, element types and load histories; the analyses were continued until numerical stability of the results was guaranteed. Figure 9 shows the distribution of the σ_{zz} component of the stress tensor at the final step in the two cases.

Figure 10 and Figure 11 instead show the ε^f_{xx} and ε^f_{zz} components of the fracture strain tensor, which reveal the distribution of cracked material in the structures and, lastly, Figure 12 shows the distribution of the isostatic lines in the structures at collapse. The limit compressive strength is attained in only a small portion of the structures. However, the high values reached by the fracture strains, as well as their distribution in the structures, reveal the presence of a large triangular shaped portion of masonry that is almost inactive, starting at about one-third the panels height on the loaded side and reaching the opposite right corner. The high values of the fracture strain ε^f_{xx} on the panel right side are induced by the concentration of vertical stresses in masonry, in the absence of horizontal restraints. These phenomena are also confirmed by the distribution of the isostatic lines (Figure 12).

MADY

MADY is a non-commercial code developed at the University of Florence (Italy) to perform nonlinear (static and dynamic) analyses of masonry structures with predominantly flexural behavior. It relies in a finite element discretization of the structures that are modeled through one-dimensional elements. To describe the constituent masonry, the nonlinear elastic constitutive equation for beams presented in Lucchesi and Pintucchi (2007) and Pintucchi and Zani (2009) is used. It is developed in terms of generalized stress and strain, accounting for the axial stress component alone and under the Euler-Bernoulli hypothesis. The material is assumed unable to withstand tensile stresses and with limited compressive strength. Specifically, the model has been developed for both solid and hollow rectangular cross-sections in order to study masonry arches as well as free-standing masonry towers.

The FE procedure used to solve the equations of flexural and axial equilibrium, which in the nonlinear range become coupled, make use of finite beam elements with three DOFs at each node: axial and transverse displacements, plus rotation. The transverse displacement and rotation are approximated using cubic interpolation, i.e. Hermite shape functions, which guarantee the continuity of both of them, while linear shape functions are adopted for the axial displacement.

To obtain the solution, standard numerical procedures – the Newton-Raphson method and the Newmark one for dynamic problems – are then used, which however require defining the element stiffness matrix. The geometric nonlinearity can also be accounted for, as detailed in Pintucchi and Zani (2009).

The model enables to perform static, pushover and nonlinear dynamic analysis with a minimum of computational effort (Pintucchi and Zani, 2014). Moreover, for these one-dimensional masonry structures, the uniqueness of the solution to static and dynamic problems has been proved in Lucchesi et al. (2012) and Lucchesi et al. (2015) respectively. Enhancements of the model can also be found in Pintucchi and Zani (2016).

The two cantilever beamns have been analyzed with MADY using 45 one-dimensional elements; increasing the number of finite elements did not lead to any significant variation of results. In the first step of the analyses the vertical loads are applied, then the lateral loads are added incrementally. Herein, the geometric nonlinearity has not been accounted for. The distribution of the axial stress at collapse is reported (both for the [10 × 40] and the [4 × 40] cantilever masonry beams) in Figure 13, while the obtained distribution of the damage is showed in Figure 14.

SMARTmasonry

SMARTmasonry is a code specifically developed at the University of Florence (Italy) to perform hybrid modelling of masonry structures, allowing the mixing in the same structural model of Discrete Elements and Finite Element discretized continuum. The latter can be possibly related to a certain micro-structural modelling (Salvatori and Spinelli, 2010). In the proposed modelling for the masonry cantilever, only rigid blocks put one on top of the other are used. The tower is discretized in 20 rigid blocks, interacting through nonlinear interfaces. The models and their deformed configuration at failure are reported in Figure 15a for the [10 × 40] cantilever beam and Figure 15b for the [4 × 40] one. More refined discretizations result in no appreciable improvements in the output quantities herein taken into consideration (first flexural bending mode and pushover capacity curve).

Kinematic effects related to the displacements of centres of gravity of each single block have been included in the co-rotational adopted model (large displacements and small deformation of the interfaces between blocks). The constitutive model for the interface is nonlinear elastic in the normal direction (with a limited compressive strength and a null tensile resistance), while it follows an elastic - perfectly plastic law along the tangential direction (according to a Mohr-Coulomb yielding criterion and non-associated flow rule). Damage in compression is related to the normal strain level (corresponding to a volume-specific fracture energy). As a matter of fact, in the present analyses the friction is large enough for not having any slip movement in the investigated structures.

In a first stage of the loading process, the self-weight is incrementally applied through a non-linear load-controlled static procedure. In the final configuration, the tangent stiffness matrix is evaluated and the modal analysis is performed. Then a nonlinear horizontal pushover analysis is performed, by using an indirect displacement-controlled static procedure, where the displacement at the top of the cantilever beam is evaluated by taking into account also the rotational contribution of the topmost block. The same model has been also used to investigate effects of material uncertainties (Salvatori et al. 2015) and of record-to-record variability in case of incremental nonlinear dynamic analyses (Marra et al. 2016).

The analyses are carried out with and without compression damage. The latter case is useful to highlight the nonlinear geometric effects (especially in the slenderer [4 × 40] structure).

Among the parameters previously described, the tensile strength has not been used, while a friction coefficient 0.4 is assumed. In the analyses where the damage is included, an ultimate strain ε_u, corresponding to a value of compressive strain ductility $\mu_\varepsilon = \varepsilon_u/\varepsilon_e = \varepsilon_u E/f_{wc} = 2.0$, is considered. This is a realistic value for historical masonry and corresponds to a volume-specific fracture energy in compression $G_{cV} = 25.0$ kJ/m^3.

The capacity curves reported in Figure 18 and Figure 19 follow the same path in the models with and without damage. Of course, in presence of damage the capacity curves terminate at smaller values of the top displacement. All curves show a progressive stiffness reduction due to the reduction of the resisting section and progressive compression crushing. When compressive failure does not occur earlier, after a peak where maximum load capacity is attained, a “softening” branch arises due to geometrically nonlinear effects (this is particularly evident for the slenderer [4 × 40] structure, in absence of damage; Figure 19). When damage is not included the conventional ultimate displacement is assumed correspondingly to a reduction of the base shear of 15% with respect to the peak. This non-realistic condition could be reached if the strain ductility were $\mu_\varepsilon = 90.1$ for the [10 × 40] structure and $\mu_\varepsilon = 7.8$ for the [4 × 40] one.

Variational Damage Model (VDM)

The variational approach to fracture was firstly proposed by Francfort and Marigo in their pioneering paper (Francfort and Marigo 1998). They supposed that the formation and propagation of cracks in brittle materials are governed by a minimization problem where the energy functional is given by the sum of a bulk term and a Griffith’s fracture term (linearly proportional to the area of the fracture surface). Later on, a variational approximation of the free-discontinuity problem (Francfort and Marigo 1998) was proposed in (Bourdin et al. 2000), essentially to bypass the numerical difficulties in representing discontinuous fields. The energy of the approximated problem is a two-field functional, depending on the displacement field $\mathbf{u}(\mathbf{x})$: $\Omega \rightarrow R^3$, and on the scalar field

$s(\mathbf{x})$: $\Omega \rightarrow [0,1]$, which represents a damage parameter, with $s = 1$ for sound material and $s = 0$ for fractured material. In an evolution process, s can only decreases, thus avoiding material healing. The form of the functional, as proposed in Pham et al. (2011), is:

$$\Theta_{\varepsilon}(\mathbf{u}, s) = \int_{\Omega} \left(\varphi(s, \nabla \mathbf{u}) + w(s) + \frac{1}{2} w_1 l \nabla s \cdot \nabla s \right) dx \qquad (2)$$

where the first term in the integral represents the elastic strain energy, which is an increasing function of both s and $\mathbf{u}$. The second term is the damage energy, a decreasing function of s, and the third term is a non-local damage contribution, with $w_1 = w(1)$ and l an intrinsic material length scale related to the width of the damaged regions. In the minimization of Eq. (2) is engaged a competition between the first integral, which is minimized for fixed $\mathbf{u}$ by $s = 0$, and the second one, minimized by $s = 1$. But the transition from $s = 0$ to $s = 1$ is associated with a non-null value of ∇s, indeed penalized in the second integral. Here, we assume:

$$\varphi(s, sym \nabla \mathbf{u}) = \frac{1}{2} s^2 \mathrm{C}[\mathrm{sym}(\nabla \mathbf{u}^{+})] \cdot \mathrm{sym}(\nabla \mathbf{u}^{+}) + \frac{1}{2} \mathrm{C}[\mathrm{sym}(\nabla \mathbf{u}^{-})] \cdot \mathrm{sym}(\nabla \mathbf{u}^{-}), \qquad (3)$$

where the displacement gradient is $\nabla \mathbf{u}^{+}$, if $\operatorname{div} \mathbf{u} > 0$ and $\nabla \mathbf{u}^{-}$, if $\operatorname{div} \mathbf{u} \leq 0$. C is the elasticity tensor of an isotropic linear elastic material. Since s affects the elastic energy only when the volume increases, the material experiences damage only in the case of tensile loadings, maintaining undamaged in the case of compressive loadings. The damage energy density is the linear function

$$w(s) = w_1(1 - s), \qquad (4)$$

where w_1 is related to the energy toughness G_c through the relation $w_1 = 3G_c / (4l\sqrt{2})$, deduced in (Pham et al. 2011). The expression relating the internal length l and the width D of the so-called process zones, i.e., that thin strip where the transition from $s = 0$ to $s = 1$ occurs, is $l = 2D / \sqrt{2}$ (see Pham et al., 2011 for details). In such a way, all the constitutive parameters are related to quantities, which can be easily measured from experiments.

The model based on the energy in Eq. (2) mainly reproduces the evolution of cleavage fracture (mode I fracture) due to tensile loadings, typical of brittle materials. However, in the last years, many variations of the functional reported in Eq. (2) were proposed to capture different fracture mechanisms. In Del Piero et al. (2007), the problem was reformulated in the most general finite elasticity setting. This extension was justified by the fact that, usually, fracture is preceded by large deformations. It has permitted to avoid problems of material interpenetration, and has furnished a more realistic description of fracture caused by compressive loads. In Lancioni and Royer-Carfagni (2009), a decomposition of the bulk energy into deviatoric and spheric parts has allowed to reproduce the formation of shear bands, and their coalescence in mode II cracks, typical of quasi-brittle materials. The behaviours under tensile and compressive loads have been differentiated in Freddi and Royer-Carfagni (2010).

The functional in Eq. (2) is numerically minimized by means of incremental energy minimization, a powerful mathematical tool used in many problems of fracture and plasticity (Del Piero et al. 2013; Lancioni 2015; Lancioni et al. 2015). At each time increment, an iterative scheme is performed, consisting in finding the local minimizers of the functional in Eq. (2), keeping s and $\mathbf{u}$ fixed, respectively. Since the functional reported in Eq. (2) is quadratic with respect to $\mathbf{u}$ and s, separately, the numerical algorithm is based on a sequential quadratic programming scheme.

Herein simulations are performed under the hypothesis of generalized plane stress. The geometric and material characteristics are assumed according the values reported in Table 1. Further quantities required by the variational model are the fracture toughness G_c=0.039 N/mm and the internal length l=750 mm. The numerical code includes a mesh refinement, which operates in those parts of the body where cracks develop. In these parts the refined mesh size is Δx=100 mm. The loading step is $\Delta q = 10^{-5}$ N/mm^2.

The obtained ductility is equal to 2.94 for the [10 × 40] beam, and 3.12 for the [4 × 40] one.

The fracture field s for different values of the load q are plotted in Figure 16 and Figure 17 for the [10 × 40] and [4 × 40] beams, respectively. The evolution of the fracture is similar in the two simulations. The fracture forms in the left bottom corner and evolves horizontally toward the central part, at the base of the wall. Then multiple cracks form on the left side and develop toward the centre of the beam base. It has been observed that, in the case of the [4 × 40] beam, the model gives a diffuse representation of the fracture, and it does not distinguish single fractures, because of the small width of the beam, comparable with the width of the damage localization zone.

Synthesis of the results and comparison

The analysis of the pushover curves allow to make comparison among them, and the following parameters were specifically estimated: i) the initial elastic stiffness (k_e); ii) the maximum base shear (V_{max}) and the correspondent load peak multiplier ($\alpha_{max}=V_{max}/W$); iii) the secant stiffness at 60% of maximum load (k_s); iv) the ultimate base shear (V_u) and the ultimate load multiplier ($\alpha_u=V_u/W$); v) the elastic displacement (d_e) and the elastic drift ($\theta_e=d_e/H$); vi) the ultimate displacement (d_u) and the corresponding ultimate drift ($\theta_u=d_u/H$); vii) the ductility ($\mu=d_u/d_e$). In addition, when the code allows for this calculation, the fundamental period (T_1) was calculated.

The initial elastic stiffness, the secant stiffness, the maximum base shear and the ultimate displacement can be directly evaluated from the pushover diagram. The ultimate displacement has been estimated as the displacement corresponding to a shear value equal to $0.85 \cdot V_{max}$ in the post-peak softening branch of the pushover curve; for those models where damage has not been taken into account, the maximum reached displacement has been considered, *i.e.* the one just before the absence of convergence in the analysis. The ultimate load multiplier, the elastic drift and the ductility were evaluated, when possible, through the estimation of the equivalent bilinear system. The bilinear system was evaluated according to an equivalent energy criterion and taking into account an initial elastic branch with a stiffness equal to the secant stiffness corresponding to a load level equal to $0.60 \cdot V_{max}$. For each quantity the mean value and the coefficient of variation (ratio between the standard deviation and the mean value) have been calculated (Table 5 and Table 6).

Comparison of the pushover curves

Results of both case studies ([10 × 40] in Table 5 and [4 × 40] in Table 6), show a good agreement with respect to the evaluation of the initial elastic stiffness, the fundamental period, and the ultimate base shear (the coefficient of variation is lower than 10%). On the contrary, differences are visible with respect to the estimation of the ultimate displacement (and drift, and consequently ductility). Comparisons of the pushover curves are reported in Figure 18 and Figure 19. As general remark, all the codes agree with respect to the evaluation of the stress conditions. With respect to the evaluation of the ultimate displacement, the numerical instruments can be grouped as follows:

a) codes 3Muri and 3DMacro evaluate the collapse load in accordance with the Italian recommendation (DM2008, 2008) based on a selected ultimate drift;
b) codes DIANA, Code ASTER, VDM, and SMARTmasonry (with damage) provide an estimation of the ultimate displacement according to the adopted damage models that allows for the evaluation of the softening branch of the pushover curve; this estimation depends on the parameters ruling the evolution of the damage (*e.g.* fracture energy);
c) the code ANSYS performs control force analysis hence is able to reproduce the initial branch of the pushover curve, but not the descending branch; then the ultimate drift is the one corresponding to the maximum base shear;
d) codes NOSA-ITACA and MADY do not have control on the ultimate displacement, which can be carried on until numeric convergence is reached. The analyses shown in the paper have been performed in force control mode and carried on until numerical stability of the results is guaranteed;
e) the code SMARTmasonry (without damage) originates a capacity curve where the reduction of strength of 85% is reached due to geometrical effects at very large values of the drift.

All the codes, but especially those adopting a damage model, provide estimations of the ultimate load quite different one from each other, highlighting a very strong dependence of the collapse displacement on the adopted constitutive model. The issue of the displacement capacity for masonry panels with dependence on their slenderness and compressive state is addressed by Orlando et al.

2016. This is a very critical point since, for instance, the Performance-Based Earthquake Engineering (PBEE) or the Capacity Spectrum Method (CSM) take into account displacements as verification parameters.

Further discussion and additional analyses

The results showed a significant dispersion associated with deformation capacity and post-peak softening branch of the pushover curves. This dispersion can significantly affect the predicted collapse performance affecting, on its turn, the confidence in structural analysis results. This demonstrated that model framework uncertainties (the uncertainties that are due to the uncertainty in the underlying science and algorithms of a model) play a key role when employed to assess the nonlinear behavior of masonry structures.

Starting from the available results, some additional analyses were performed in order to better characterize the ultimate displacement of the two examined beams and to estimate the reliability level connected to the epistemic uncertainty.

Firstly, a mean collapse curve has been determined, by considering the *i*-th average load multiplier $\alpha_{i,avg}$ obtained among the m_i analyses still running at each of the *i*-th displacement level d_i, *i.e.*

$$\alpha_{i,avg} = \frac{1}{m_i}\sum_{j=1}^{m_i} \alpha_j(d_i) \qquad (5)$$

with:

$$m_i = \sum_{j=1}^{n} \delta_{ij}, \qquad \delta_{ij} = \begin{cases} 1 & if \quad d_{max,j} \geq d_i \\ 0 & if \quad d_{max,j} < d_i \end{cases} \qquad (6)$$

where n=10 (in case of SMARTmasonry, only the case with damage has been considered) is the number of the approaches, $d_{max,j}$ the maximum displacement estimated for the *j*-th approach and $\alpha_j(d_i)$ the load multiplier of the *j*-th approaches at the *i*-th displacement d_i.

As, for a given force value, each analysis provides different values of the displacement d (some analyses are force controlled, so that no fixed values for displacements are assumed), all curves have been resampled at given values of displacements d_i; the spacing $\Delta_i = d_{i+1} - d_i, \;\; i = 1, \cdots, N$ has been selected as 1/100 of the maximum displacement obtained among all curves (N=100).

At the same time, a curve reporting for each displacement level d_i the value of the number m_i of analyses still considering an ultimate displacement $d_{max,j}$ higher than the considered displacement level d_i has been evaluated. Once the obtained histogram has been normalized with respect to the total number n of the performed analysis, it can be fitted in a way of representing an exceedance probability distribution of the d_i values (reliability curve); the obtained curve then represents the reliability level of the displacement level d_i. In other words, if m_i analyses out of n assert that this displacement can be reached and if the same degree of soundness is given to each individual analysis, it means that this value can be viewed as the value which has a probability

$$Prob[d_{max} \geq d_i] = \frac{m_i}{n} \tag{7}$$

of being exceeded. The value corresponding to an exceedance probability of 0.50 (median) has been selected as the most probable collapse value for the examined structures. As shown in Figure 20, the two examined cases exhibit a similar behavior and the proposed curve can be retained as a reliability function for the ultimate displacement; the spreadiness of the distribution makes evidence of the large variability of this parameter.

A second analysis has been performed by analyzing the standard deviation values σ_i at each d_i level; the parameter accounts for the dispersion of the results given by the various analyses at an assigned displacement level, and it is meaningful only if $m_i > 2$.

The obtained σ_i values have then been normalized with respect to mean value $\alpha_{i,avg}$ previously determined, then obtaining the function describing the evolution of the Coefficient of Variation (CoV) at increasing displacement levels:

$$(CoV)_i = \frac{\sigma_i}{\alpha_{i,avg}} \tag{8}$$

In Figure 21, the mean curve and the curves corresponding to $\alpha_{i,avg} + \sigma_i$ and $\alpha_{i,avg} - \sigma_i$ have been reported. In the same graphs, the values of $(\text{CoV})_i$ as a function of d_i have been reported, too.

Due to the strong analogy between the graphs related to [10 × 40] and [4 × 40] beams, a normalization has then been proposed, by scaling the ordinates and the abscissae of the two curves with respect to the values at the elastic limit, *i.e.* to the values α_{el} and d_{el} corresponding to the end of an equivalent elastic branch. The latter has been determined, for each analysis, as the displacement value at which the difference between the actual force level and the one obtained by using the elastic stiffness (*i.e.* the value corresponding to the initial tangent stiffness) overpass a given threshold fixed at 5%.

With respect to this normalization, the two curves show a very similar trend (as reported in Figure 22). It can be stated that both the analyses give the same normalized ultimate load level, which can be estimated as $\alpha_{avg} / \alpha_{el} \cong 1.7$ (*i.e.* the ultimate load is 1.7 times the load at the elastic level), while the ultimate normalized displacement, which plays the role of the ductility of the beams, depends on the geometry; in the investigated cases, the average ductility (with respect to the performed analyses) can be assumed equal to about $d/d_{el} \cong 6$.

It is indeed interesting to observe that, in normalized form, the evolution of the coefficient of variation with respect to the displacement level has the same shape for both cases, so a common expression can be proposed as a reasonable approximation of the obtained results:

$$(CoV)_i = 0.025 + 0.01\frac{d_i}{d_{el}} \tag{9}$$

or, in an equivalent form:

$$\sigma_i = \sigma(V_i/V_{el}) = \frac{V_i}{V_{el}}\left[0.025 + 0.01\frac{d_i}{d_{el}}\right] \tag{10}$$

The obtained line is reported as a dashed line in the graphs in Figure 22.

This result is quite relevant as it assesses that the obtained average curve has a growing standard deviation (*i.e.* a lowering confidence level) which is proportional to both the load level and the displacement level.

The same level of soundness can be attributed to the result of a single analysis to account for the epistemic uncertainty. As a first approximation, the obtained value for the standard deviation could be attributed to each of the curves obtained by the different analyses to take into account the uncertainties related to the specific mechanical and numerical model.

Concluding remarks

The paper reported the results of a blind benchmark aimed at comparing the results obtained with different analytical models and/or numerical analysis techniques (macro-elements, equivalent frame, finite elements, energy approach, etc.) for the assessment of the structural behavior of a series of slender masonry elements under increasing horizontal loads. The comparison, aimed at deepening the effects of the so-called model framework uncertainties, showed a good agreement in terms of all the main parameters that define the capacity curve, except for the ultimate drift, whose determination is crucial to the audit: it is subject to uncertainties that are reflected on the entire chain of seismic risk assessment.

As a matter of fact, all the approaches, but especially those adopting a damage model, provide estimations of the ultimate load quite different one from each other, highlighting a very strong dependence of the collapse displacement on the employed constitutive model. This is a very critical point, since deformation capacity has a direct consequence in decision-making, because both the assessment (or retrofitting) of existing structures and the design of new buildings depend on seismic capacity predictions: for instance, the Performance-Based Earthquake Engineering (PBEE) or the Capacity Spectrum Method (CSM) take into account displacements as verification parameters. This enlightens that, at the present state of knowledge, engineering expert judgment still plays a strategic role to assess the seismic safety of masonry structures when a nonlinear numerical code is employed.

ACKNOWLEDGEMENTS

The authors kindly acknowledge the Region of Tuscany that financially supported the research (theme PAR FAS 2007-2013 - CIPE n°166/2007 - line 1.1.a.3: Science and Technology for the preservation and enhancement of cultural heritage).

REFERENCES

3DMacro [Computer software]. Torino, Italy. Internet site: http://www.stadata.com.

3Muri [Computer software]. Catania, Italy. Internet site: http://www.murature.com.

Adam, J.M. Brencich, A, Hughes, T.G. and Jefferson T. (2010). “Micromodelling of eccentrically loaded brickwork: Study of masonry wallettes.” Engineering Structures, 32(5), 1244-1251. doi: 10.1016/j.engstruct.2009.12.050.

ANSYS [Computer software]. Canonsburg, PA, USA. Internet site: http://www.ansys.com.

Asteris, P.G., Sarhosis, V., Mohebkhah, A., Plevris, V., Papaloizou, L., Komodromos, P., and Lemos, J.V. (2015). “Numerical Modeling of Historic Masonry Structures.” In Asteris, P.G., and Plevris, V. (eds), Handbook of Research on Seismic Assessment and Rehabilitation of Historic Structures (2 Volumes). IGI Global, 213-256. doi: 10.4018/978-1-4666-8286-3.ch007.

Bartoli, G., Betti, M., and Vignoli A. (2016). “A numerical study on seismic risk assessment of historic masonry towers: a case study in San Gimignano.” Bulletin of Earthquake Engineering, 14(6), 1475-1518. doi: 10.1007/s10518-016-9892-9.

Bennati, S., Nardini, L., and Salvatore, W. (2005). "Dynamic Behavior of a Medieval Masonry Bell Tower. II: Measurement and Modeling of the Tower Motion." Journal of Structural Engineering, 131(11), 1656-1664. doi: 10.1061/(ASCE)0733-9445(2005)131:11(1656).

Betti, M., Galano, L., Petracchi, M., and Vignoli A. (2015). “Diagonal cracking shear strength of unreinforced masonry panels: a correction proposal of the b shape factor.” Bulletin of Earthquake Engineering, 13(10), 3151-3186. doi: 10.1007/s10518-015-9756-8.

Betti, M., Galano, L., and Vignoli, A. (2016). “Finite element modelling for seismic assessment of historic masonry buildings.” In D'Amico, S. (ed), *Earthquakes and Their Impact on Society. Springer Natural Hazards*, 377-415. doi: 10.1007/978-3-319-21753-6_14.

Binante, V., Girardi, M., Padovani, C., Pagni, A., and Pasquinelli G. (2012). “The NOSA-ITACA code for the modelling of the structural behaviour of historic masonry constructions.”

Proceedings of the 5th International Congress on "Science and Technology for the Safeguard of Cultural Heritage in the Mediterranean Basin", 2011, Istanbul, Turkey.

Bourdin, B., Francfort, G.A., and Marigo, J.J. (2000). “Numerical experiments in revisited brittle fracture.” Journal of the Mechanics and Physics of Solids, 48(4), 797-826. doi:10.1016/S0022-5096(99)00028-9.

Bradley, B.A. (2010). “Epistemic Uncertainties in Component Fragility Functions.” Earthquake Spectra, 26(1), 41–62. doi: http://dx.doi.org/10.1193/1.3281681.

Caliò, I., Marletta, M., and Pantò, B. (2005). “A simplified model for the evaluation of the seismic behaviour of masonry building.” Proceedings of the 10th International Conference on Civil, Structural and Environmental Engineering Computing, Civil-Comp Press, Stirlingshire, UK, Paper 195. doi: 10.4203/ccp.81.195.

Caliò, I., Marletta, M., and Pantò B. (2008). “A discrete element approach for the evaluation of the seismic response of masonry buildings.” Proceedings of the 14th World Conference on Earthquake Engineering, 2008, Beijing, China.

Caliò, I., Marletta, M., and Pantò B. (2012). “A new discrete element model for the evaluation of the seismic behaviour of unreinforced masonry buildings.” Engineering Structures, 40, 327-338. doi:10.1016/j.engstruct.2012.02.039.

Cattari, S., Galasco, A., Lagomarsino, S., and Penna, A. (2004). “Analisi non lineare di edifici in muratura con il programma TREMURI”. Atti del XI Congresso Nazionale L’Ingegneria Sismica in Italia, ANIDIS, Genova, Italy (in Italian)

Chiostrini, S., Galano, L., and Vignoli, A. (2003). “In Situ Shear and Compression Tests in Ancient Stone Masonry Walls of Tuscany, Italy.” Journal of Testing and Evaluation, 31(4), 289-304. doi: 10.1520/JTE12175J.iI

Code ASTER [Computer software]. Paris, France. Internet site: http://www.code-aster.org.

Del Piero G. (1989). “Constitutive equation and compatibility of the external loads for linear elastic masonry-like materials.” Meccanica, 24(3), 150-162. doi: 10.1007/BF01559418.

Del Piero, G., Lancioni, G., and March, R. (2007). “A variational model for fracture mechanics: numerical experiments.” Journal of the Mechanics and Physics of Solids, 55, 2513–2537. doi: 10.1016/j.jmps.2007.04.011.

Del Piero, G., Lancioni, G., March, R. (2013). “A diffuse cohesive energy approach to fracture and plasticity: the one-dimensional case”, Journal of Mechanics of Materials and Structures, 8(2-4), 109-151. doi: 10.2140/jomms.2013.8.109.

Der Kiureghian, A., and Ditlevsen, O. (2009). “Aleatory or epistemic? Does it matter?” Structural Safety, 31, 105-112. doi: 10.1016/j.strusafe.2008.06.020.

DIANA [Computer software]. Delft, Netherlands. Internet site: http://dianafea.com.

Di Pasquale, S. (1992). “New trends in the analysis of masonry structures.” Meccanica, 27, 173-184. doi: 10.1007/BF00430043.
Drucker, D. and Prager, W. (1952). “Soil mechanics and plastic analysis or limit design.” Quarterly of Applied Mathematics, 10(2), 157-165.
Francfort, G.A., and Marigo, J.J. (1998). “Revisiting brittle fracture as an energy minimization problem.” Journal of the Mechanics and Physics of Solids, 46(8), 1319-1342. doi: 10.1016/S0022-5096(98)00034-9.
Freddi, F., and Royer-Carfagni, G. (2010). “Regularized variational theories of fracture: A unified approach.” Journal of the Mechanics and Physics of Solids, 58(8), 1154–1174. doi: 10.1016/j.jmps.2010.02.010.
Galano, L., and Vignoli, A. (2001). “Resistenza a Taglio di Murature di Pietrame: Analisi Comparata della Rappresentatività di Tipiche prove di Taglio in Situ”. Atti del X Congresso Nazionale L’Ingegneria Sismica in Italia, ANIDIS, Potenza/Matera, Italy (in Italian).
Ginovart, J.L., Costa, A. and Fortuny G. (2013). “Assessment and restoration of a masonry dome in the cathedral of Tortosa enclosure.” Proceedings of the 13th International Conference on “Studies, Repairs and Maintenance of Heritage Architecture (STREMAH2013)”, 2013, New Forest, UK. doi: 10.2495/STR130331.
Girardi, M., Padovani, C. and Pellegrini, D. (2015). “The NOSA-ITACA code for the safety assessment of ancient constructions: A case study in Livorno.” Advances in Engineering Software, 89, 64-76. doi: 10.1016/j.advengsoft.2015.04.002.
Helton, J.C., and Oberkampf, W.L. (2004). “Guest Editorial to the Special Issue: Alternative Representations of Epistemic Uncertainty.” Reliability Engineering and System Safety, 85(1-3), 1-10. doi: 10.1016/j.ress.2004.03.001.
Hordijk, D.A. (1991). “Local Approach to Fatigue of Concrete.” PhD Thesis, Delft University of Technology. (http://repository.tudelft.nl/islandora/object/uuid:fa87147b-8201-47ed-83d7-b812b09c5fbb?collection=research).
Lagomarsino S. (2011). “Valutazione della sicurezza sismica del patrimonio architettonico in muratura.” Atti del XIV Congresso Nazionale L’Ingegneria Sismica in Italia, ANIDIS, Bari, Italy (in Italian).
Lagomarsino, S., Penna, A., Galasco, A., and Cattari, S. (2013). “TREMURI program: An equivalent frame model for the nonlinear seismic analysis of masonry buildings.” Engineering Structures, 56, 1787-1799. doi: 10.1016/j.engstruct.2013.08.002.
Lancioni, G., and Royer-Carfagni, G. (2009). “The Variational Approach to Fracture Mechanics. A Practical Application to the French Panthéon in Paris.” Journal of Elasticity, 95, 1-30. doi: 10.1007/s10659-009-9189-1.

Lancioni, G. (2015). “Modeling the Response of Tensile Steel Bars by Means of Incremental Energy Minimization.” Journal of Elasticity, 121(1), 25-54. doi: 10.1007/s10659-015-9515-8.

Lancioni, G., Yalcinkaya, T., and Cocks, A. (2015). “Energy based non-local plasticity models for deformation patterning, localization and fracture.” Proceedings of the Royal Society A, 471: 20150275. Doi :10.1098/rspa.2015.0275.

Lin, Y.K. (1967). *Probabilistic theory of structural dynamics*. Mc-Graw Hill.

Lin, Y.K., and Cai, G.C. (1995). *Probabilistic structural dynamics. Advanced theory and applications*. Mc-Graw Hill.

Lourenço, P.B., Rots, J.C., and Blaauwendraad, J. (1998). “Continuum model for masonry: parameter estimation and validation.” ASCE Journal of Structural Engineering, 124(6), 642-652. doi: 10.1061/(ASCE)0733-9445(1998)124:6(642).

Lucchesi, M., and Pintucchi, B. (2007). “A numerical model for non-linear dynamics analysis of masonry slender structures.” European Journal of Mechanics A/Solids, 26, 88-105. doi: 10.1016/j.euromechsol.2006.02.005.

Lucchesi, M., Padovani, C., Pasquinelli, G., and Zani N. (2008). “*Masonry constructions: mechanical models and numerical applications*”, Series: Lecture Notes in Applied and Computational Mechanics, Vol. 39, Berlin Heidelberg, Springer-Verlag.

Lucchesi, M., Silhavy, M., and Zani, N. (2012). “Equilibrium problems and limit analysis of masonry beams.” Journal of Elasticity, 106, 165-188. doi: 10.1007/s10659-011-9318-5.

Lucchesi, M., Pintucchi, B., Silhavy, M., and Zani, N. (2015). “On the dynamics of viscous beams.” Continuum Mechanics and Thermodynamics, 27(3), 349-365. doi:10.1007/s00161-014-0352-y.

Maio, R., Vicente, R., Formisano, A., and Varum, H. (2015). “Seismic vulnerability of building aggregates through hybrid and indirect assessment techniques.” Bulletin of Earthquake Engineering, 13(10), 2995–3014. doi: 10.1007/s10518-015-9747-9.

Marra, A.M., Salvatori, L., Spinelli, P., and Bartoli, G., (2016). “Incremental dynamic and nonlinear static analyses for seismic assessment of medieval masonry towers.” Journal of Performance of Constructed Facilities.

Mazars, J.M., and Pijaudier-Cabot, G. (1989). “Continuum Damage Theory. Application to Concrete.” ASCE Journal of Engineering Mechanics, 115(2), 345-365. doi: 10.1061/(ASCE)0733-9399(1989)115:2(345).

Mendes, N., and Lourenço, P.B. (2014). “Sensitivity analysis of the seismic performance of existing masonry buildings.” Engineering Structures, 80(1), 137-146. doi: 10.1016/j.engstruct.2014.09.005.

Most, T (2011). “Assessment of structural simulation models by estimating uncertainties due to model selection and model simplification.” Computers and Structures, 89, 1664-1672. doi: 10.1016/j.compstruc.2011.04.012.

Munjiza A. (2004). The Combined Finite-Discrete Element Method. Wiley, New York. ISBN: 9780470841990.

NTC2008. (2008). “Decreto Ministeriale del Ministero delle Infrastrutture e dei Trasporti del 14/01/2008. Nuove Norme Tecniche per le Costruzioni.” S.O. n.30 alla G.U. del 4.2.2008, No. 29 (in Italian).

Orlando, M., Salvatori, L., Spinelli, P., and De Stefano, M. (2016). “Displacement capacity of masonry piers: parametric numerical analyses versus international building codes.” Bulletin of Earthquake Engineering, 14, 2259-2271. doi: 10.1007/s10518-016-9903-x.

Pan, Q., Grimmelsman, K., Moon, F., and Aktan E. (2011). “Mitigating Epistemic Uncertainty in Structural Identification: Case Study for a Long-Span Steel Arch Bridge.” Journal of Structural Engineering, 137(1), 1-13. doi: 10.1061/(ASCE)ST.1943-541X.0000248.

Pham, K., Amor, H., Marigo, J.J., and Maurini, C. (2011). “Gradient damage models and their use to approximate brittle fracture”, International Journal of Damage Mechanics, 20, 618-652.

Pieraccini, M., Dei, D., Betti, M., Bartoli, G., Tucci, G., and Guardini, N. (2014). “Dynamic identification of historic masonry tower through and expeditious and no-contact approach: Application to the “Torre del Mangia” in Siena (Italy).” Journal of Cultural Heritage, 15(3), 275–282. doi: 10.1016/j.culher.2013.07.006.

Pintucchi, B., and Zani, N. (2009). “Effects of material and geometric non-linearities on the collapse load of masonry arches.” European Journal of Mechanics A/Solids, 28, 45-61. doi: 10.1016/j.euromechsol.2008.02.007.

Pintucchi, B., and Zani, N. (2014). “Effectiveness of nonlinear static procedures for slender masonry towers.” Bulletin of Earthquake Engineering, 12(6), 2531-2556. doi: 10.1007/s10518-014-9595-z.

Pintucchi, B., and Zani, N. (2016). “A simple model for performing nonlinear static and dynamic analyses of unreinforced and FRP-strengthened masonry arches.” European Journal of Mechanics A/Solids, 59, 210-231. doi: 10.1016/j.euromechsol.2016.03.013.

Porcelli, M., Binante, V., Girardi, M., Padovani, C. and Pasquinelli, G. (2015). “A solution procedure for constrained eigenvalue problems and its application within the structural finite-element code NOSA-ITACA.” Calcolo, 52(2), 167-186.

Salvatori, L., Marra, A.M., Bartoli, G., and Spinelli P. (2015). “Probabilistic seismic performance of masonry towers: General procedure and a simplified implementation.” Engineering Structures, 94, 82-95. doi: 10.1016/j.engstruct.2015.02.017.

Salvatori, L. and Spinelli P. (2010). “Microstructural, homogenised, and multiscale models for masonry structures based on rigid blocks.” Proceedings of 8-IMC, Dresden, Germany.

SMARTmasonry [Computer software]. Internet site: http://www.smartmasonry.it

Tarque, N., Camata, G., Spacone, E, Varum, H. and Blondet, M. (2014). “Nonlinear Dynamic Analysis of a Full-Scale Unreinforced Adobe Model.” Earthquake Spectra, 30(4), 1643-1661. doi: 10.1193/022512EQS053M.

Theodossopoulos D., and Sinha B. (2013). “A review of analytical methods in the current design processes and assessment of performance of masonry structures.” Construction and Building Materials, 41, 990-1001. doi: 10.1016/j.conbuildmat.2012.07.095.

Thorenfeldt, E., Tomaszewicz, A., and Jensen J.J. (1987). “Mechanical properties of high-strength concrete and applications in design.” Proceedings of the Symposium on Utilization of High-Strength Concrete (Stavanger, Norway), Tapir, Trondheim, Norway.

Tondelli, M., Rota, M., Penna, A., and Magenes, G. (2012). “Evaluation of Uncertainties in the Seismic Assessment of Existing Masonry Buildings.” Journal of Earthquake Engineering, 16(1), 36-64. doi: 10.1080/13632469.2012.670578.

Valente, M., and Milani, M. (2016). “Non-linear dynamic and static analyses on eight historical masonry towers in the North-East of Italy.” Engineering Structures, 114, 241-270. doi: 10.1016/j.engstruct.2016.02.004.

Willam, K.J., and Warnke, E.P. (1975). “Constitutive model for the triaxial behaviour of concrete”. IABSE Seminar on Concrete Structures Subjected to Triaxial Stresses, Bergamo, Italy.

Table 1. Mechanical parameters: E_w (elastic modulus); ν (Poisson's coefficient); f_{wc} (uniaxial compressive strength); f_{wt} (uniaxial tensile strength); τ_k (characteristic shear strength).

E_w (N/mm^2)	ν	f_{wc} (N/mm^2)	f_{wt} (N/mm^2)	τ_k (N/mm^2)
1500	0.25	5.00	0.24	0.293

Table 2. DIANA model: additional mechanical parameters.

Poisson's coefficient ν (-)	Fracture energy G_f (N/m)	crack bandwidth h (m)	shear retention factor β (-)
0.00	38.97	0.75	0.35

Table 3. Code ASTER model: additional mechanical parameters required to define the Mazars model.

Parameter	Value
κ_0 damage threshold [-]	$3.2\ 10^{-5}$
A_c shape coefficient (compression asymptote) [-]	1.0
B_c shape coefficient (compression peak) [-]	$2.2\ 10^{3}$
A_t shape coefficient (tensile asymptote) [-]	0.8
B_t shape coefficient (tensile peak) [-]	$2\ 10^{4}$
β coupling coefficient of the damage in compression and tension [-]	1.06

Table 4. ANSYS model: additional parameters for DP yield criterion and WW failure surface.

Nonlinear Material parameters	Model 1 (DP&WW)	Model 2 (WW)
Drucker-Prager yield criterion parameters		
c (cohesion)	0.5384 MPa	/
η (flow angle)	65.69°	/
φ (friction angle)	43.79°	/
f_{cDP} (uniaxial compressive strength)	5.0 MPa	/
f_{tDP} (uniaxial tensile strength)	0.34 MPa	/
Willam-Warnke failure criterion parameters		
F_c (uniaxial compressive strength)	6 MPa	5 MPa
F_t (uniaxial tensile strength)	0.24 MPa	0.24 MPa
β_c (shear transfer coeff. for close cracks)	0.75	0.75
β_t (shear transfer coeff. for open cracks)	0.25	0.25

Table 5. Cantilever beam [10 × 40]. Fundamental period (T_1), initial elastic stiffness (k_e), peak multiplier ($\alpha_{max}=V_{max}/P$), ultimate *drift* ($\theta_u=d_u/h$), secant stiffness (k_s), elastic *drift* ($\theta_e=d_e/h$), ductility ($\mu=d_u/d_e$), ultimate load multiplier ($\alpha_u=V_u/P$).

		3Muri	3DMacro	DIANA	Code ASTER	ANSYS		NOSA	MADY	VDM	SMARTmasonry		*Mean*	*CoV*
						(1)	(2)				(3)	(4)		
T_1	[s]	0.99	-	1.13	1.13	1.14	1.14	1.33	1.09	-	1.14	1.14	*1.14*	*0.0768*
k_e	[kN/mm]	34.78	36.50	37.22	36.80	37.10	37.23	36.79	39.06	37.00	36.32	36.32	*36.83*	*0.0275*
α_{max}	[-]	0.193	0.212	0.195	0.212	0.208	0.199	0.178	0.217	0.203	0.206	0.206	*0.203*	*0.0542*
θ_u	[‰]	8.30	4.03	8.30	14.10	10.63	6.90	11.31	18.46	5.00	8.60	51.19	*13.35*	*0.9888*
k_s	[kN/mm]	33.52	35.90	37.15	-	-	-	35.11	-	-	30.66	30.65	*33.83*	*0.0806*
θ_e	[‰]	2.44	2.46	2.18	1.30	5.28	1.32	2.16	1.63	1.70	2.74	2.69	*2.35*	*0.4661*
μ	[-]	3.39	1.64	3.80	10.85	8.05	5.24	5.24	11.33	2.94	3.08	19.06	*6.78*	*0.7655*
α_u	[-]	0.182	0.196	0.184	0.212	0.208	0.199	0.168	0.209	0.203	0.194	0.187	*0.195*	*0.0692*

Note: (1) DP&WW criteria; (2) WW criterion; (3) with damage; (4) without damage.

Table 6. Cantilever beam [4 × 40]. Fundamental period (T_1), initial elastic stiffness (k_e), peak multiplier ($\alpha_{max}=V_{max}/P$), ultimate *drift* ($\theta_u=d_u/h$), secant stiffness (k_s), elastic *drift* ($\theta_e=d_e/h$), ductility ($\mu=d_u/d_e$), ultimate load multiplier ($\alpha_u=V_u/P$).

		3Muri	3DMacro	DIANA	Code ASTER	ANSYS		NOSA	MADY	VDM	SMARTmasonry		*Mean*	*CoV*
						(1)	(2)				(3)	(4)		
T_1	[s]	2.25	-	2.73	2.68	2.76	2.76	2.73	2.71	-	2.84	2.84	*2.70*	*0.0659*
k_e	[kN/mm]	2.38	2.43	2.48	2.24	2.48	2.48	2.48	2.50	2.53	2.29	2.29	*2.42*	*0.0415*
α_{max}	[-]	0.076	0.0756	0.084	0.071	0.082	0.077	0.073	0.087	0.088	0.068	0.068	*0.077*	*0.0923*
θ_u	[‰]	15.10	10.00	22.46	11.38	18.21	12.35	25.25	43.80	15.00	24.61	34.61	*21.16*	*0.4968*
k_s	[kN/mm]	2.31	2.43	2.47	-	-	-	-	-	-	2.13	2.13	*2.29*	*0.0701*
θ_e	[‰]	5.55	5.04	5.64	4.23	3.33	3.31	5.00	6.50	4.80	5.43	5.25	*4.92*	*0.1973*
μ	[-]	2.72	1.98	3.98	2.69	5.47	3.73	5.00	6.73	3.12	4.53	6.59	*4.23*	*0.3759*
α_u	[-]	0.071	0.076	0.079	0.071	0.082	0.077	0.068	0.083	0.080	0.065	0.063	*0.074*	*0.0930*

Note: (1) DP&WW criteria; (2) WW criterion; (3) with damage; (4) without damage.

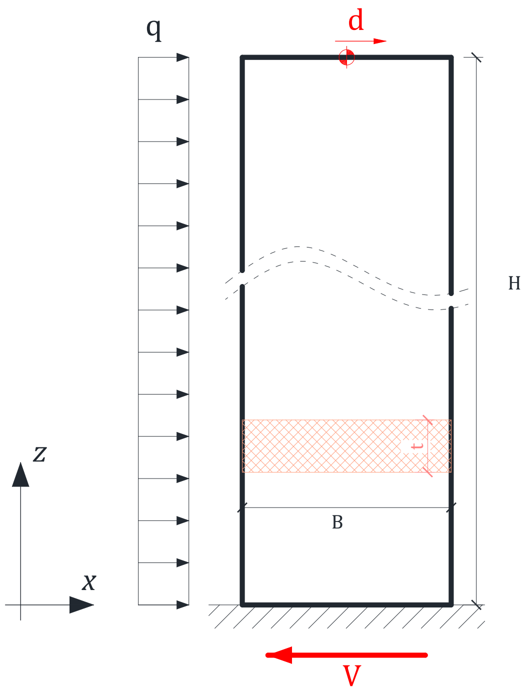

Figure 1. The cantilever masonry beam.

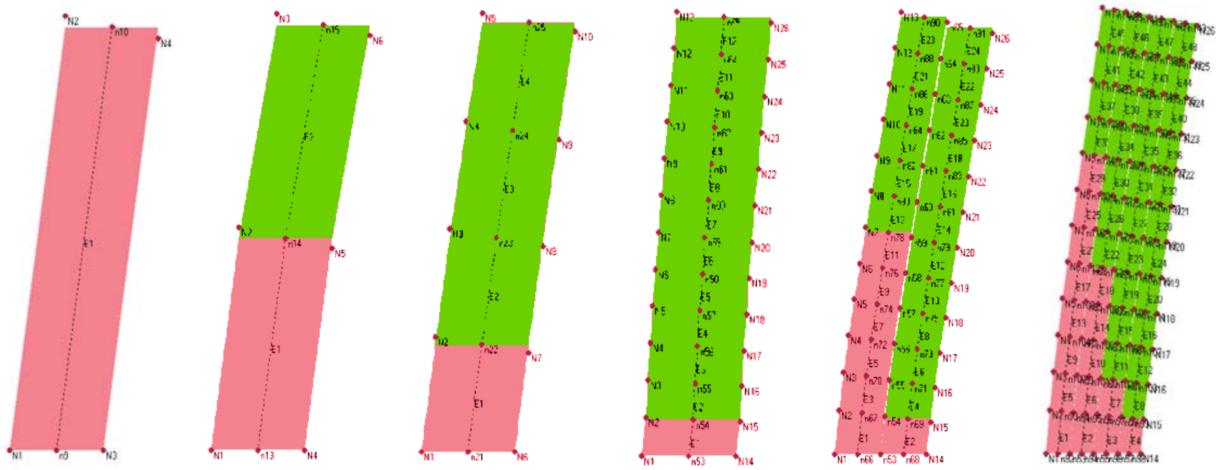

(a) (b) (c) (d) (e) (f)

Figure 2. 3Muri: discretization of the [10 × 40] cantilever masonry beam (pink elements denote those collapsed at the end of the pushover analysis).

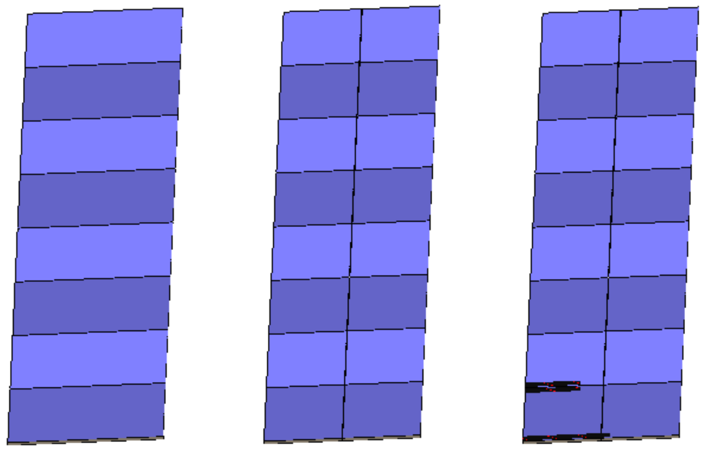

(a) (b) (c)

Figure 3. 3DMacro: discretization of the [10 × 40] cantilever masonry beam and corresponding collapse configurations.

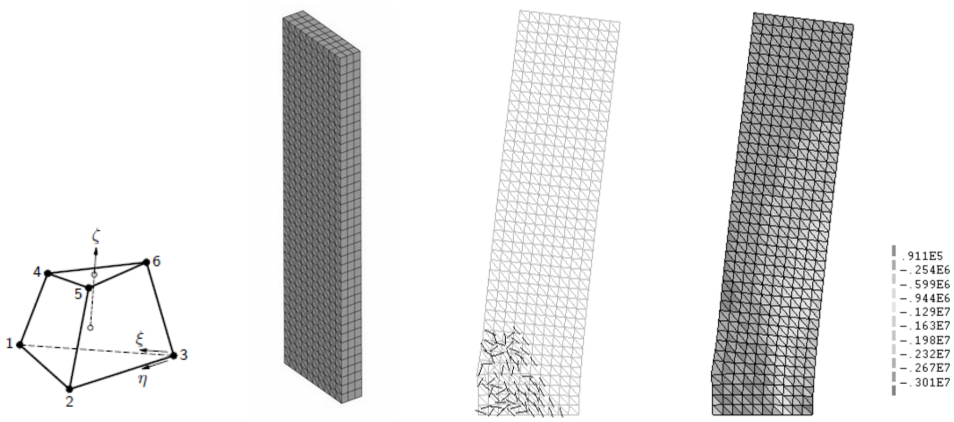

(a) (b) (c)

Figure 4. DIANA: (a) 6-node isoparametric TP18L element; (b) discretization of the [10 × 40] cantilever masonry beam; (c) cracking pattern and vertical stresses corresponding to the maximun base shear for the [10 × 40] cantilever beam.

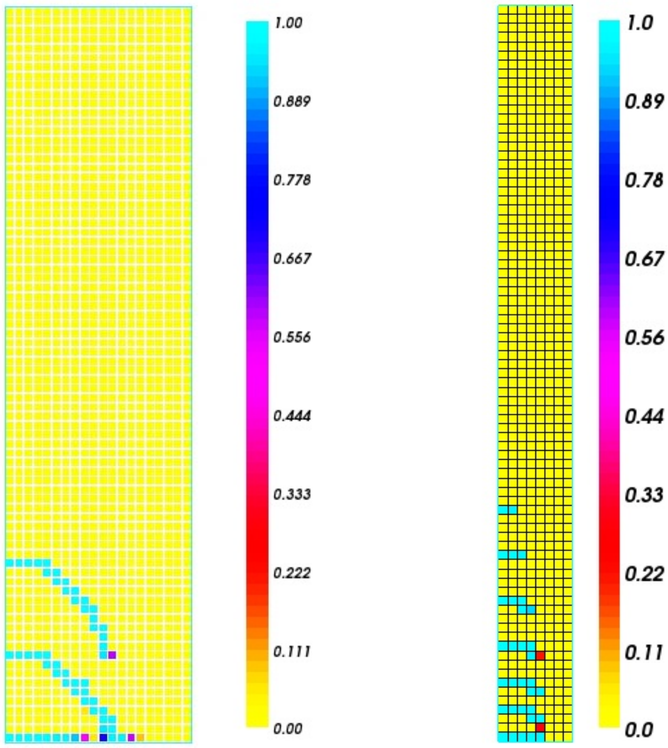

(a) (b)

Figure 5. Code ASTER: damage map at collapse for (a) [10 × 40] and (b) [4 × 40] cantilever masonry beams.

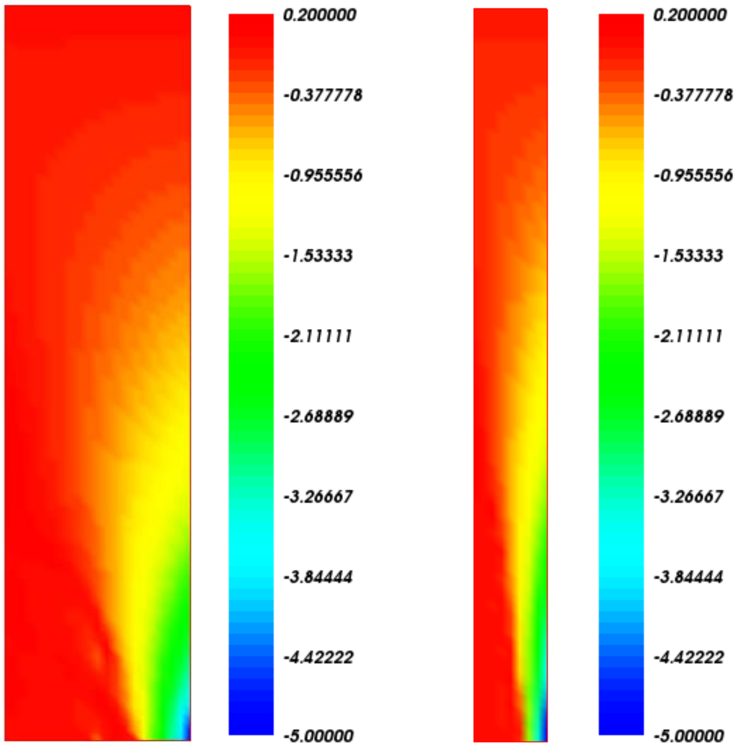

(a) (b)

Figure 6. Code ASTER: principal compressive stresses (MPa) at collapse for (a) [10 × 40] and (b) [4 × 40] cantilever masonry beams.

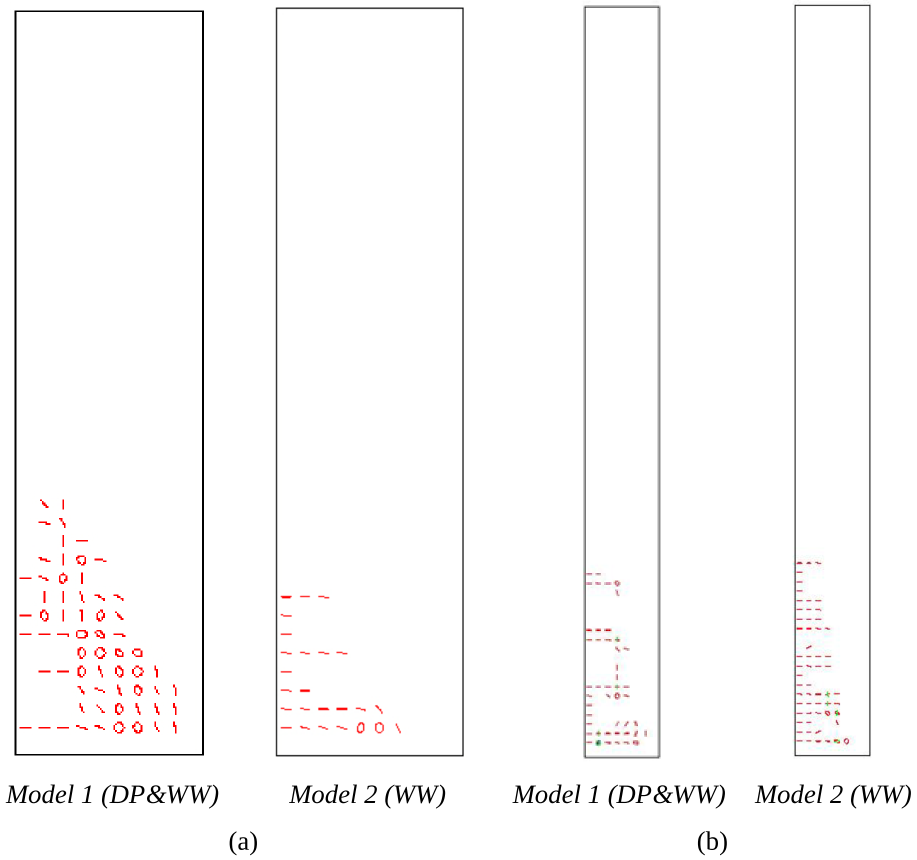

Figure 7. ANSYS: cracking pattern at collapse for (a) [10 × 40] and (b) [4 × 40] cantilever masonry beams.

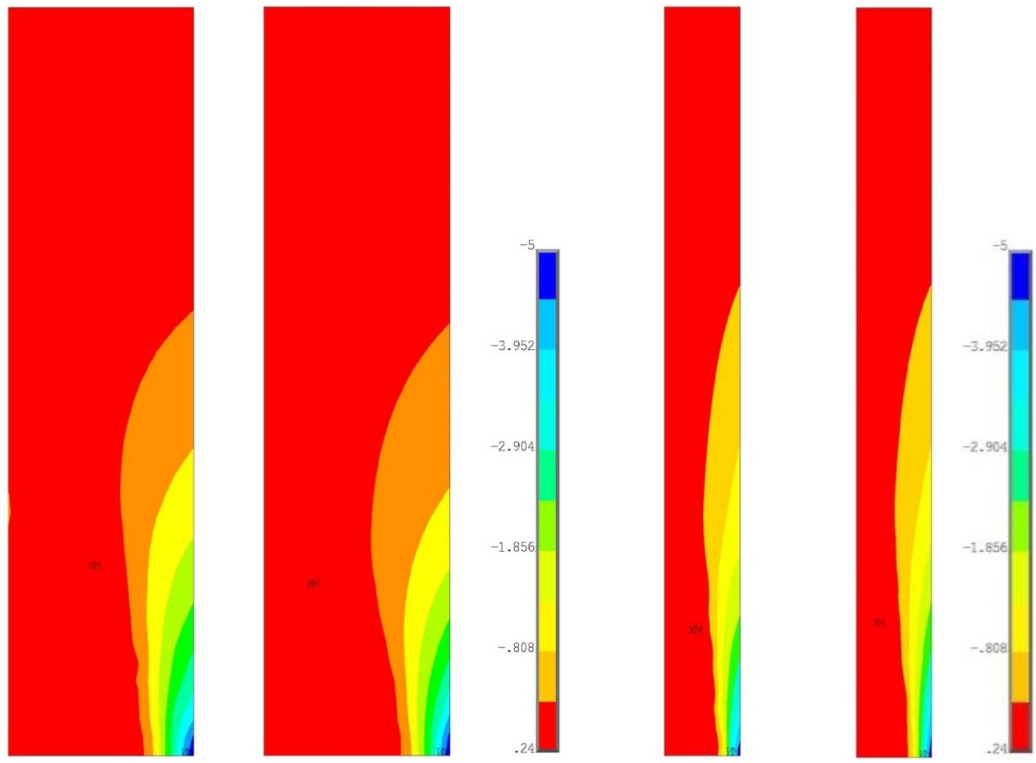

Model 1 (DP&WW) *Model 2 (WW)* *Model 1 (DP&WW)* *Model 2 (WW)*

(a) (b)

Figure 8. ANSYS: principal compressive stresses (MPa) at collapse for (a) [10 × 40] and (b) [4 × 40] cantilever masonry beams.

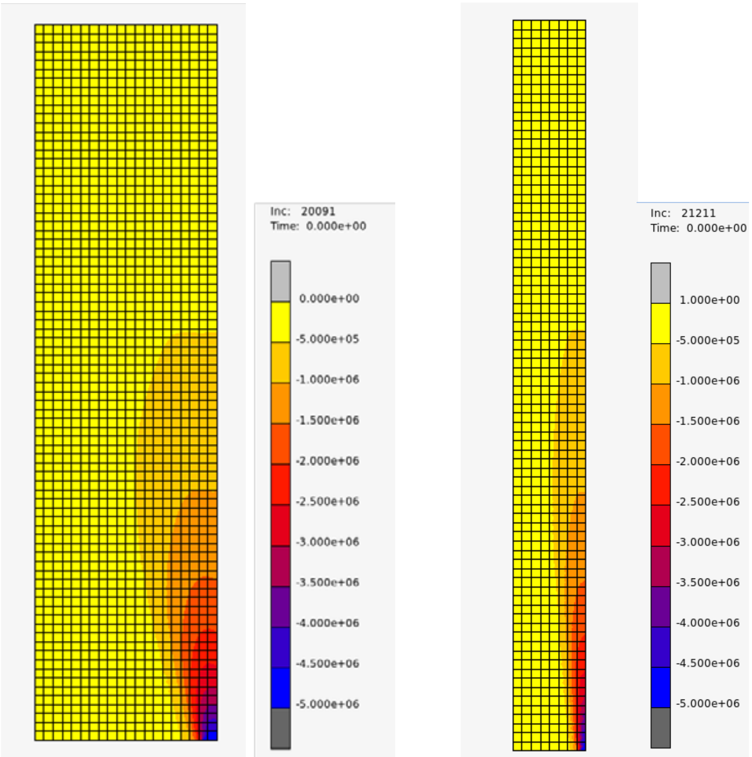

(a) (b)

Figure 9. NOSA-ITACA: distribution of the σ_{zz} (N/m^2) stress tensor component at collapse obtained for (a) [10 × 40] and (b) [4 × 40] cantilever masonry beams.

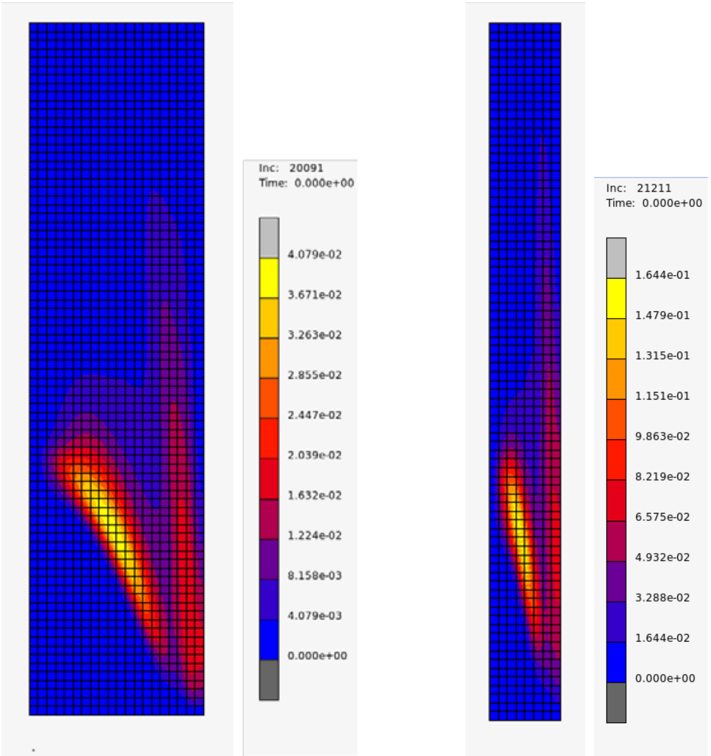

(a) (b)

Figure 10. NOSA-ITACA: distribution of the ε^{f}_{xx} component of the fracture strain tensor at collapse obtained for (a) [10 × 40] and (b) [4 × 40] cantilever masonry beams.

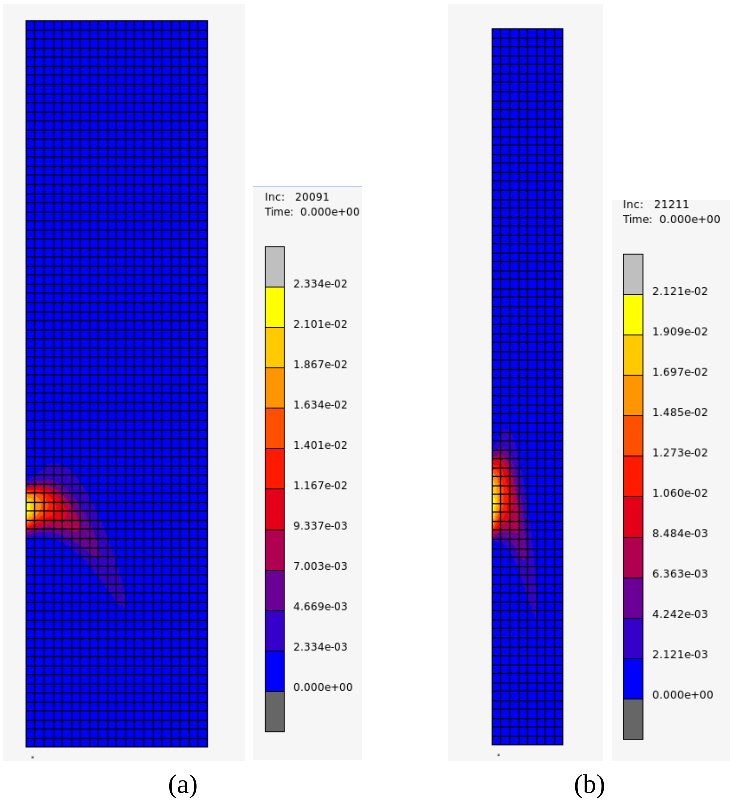

Figure 11. NOSA-ITACA: distribution of the ε^{f}_{zz} component of the fracture strain tensor at collapse obtained for (a) [10 × 40] and (b) [4 × 40] cantilever masonry beams.

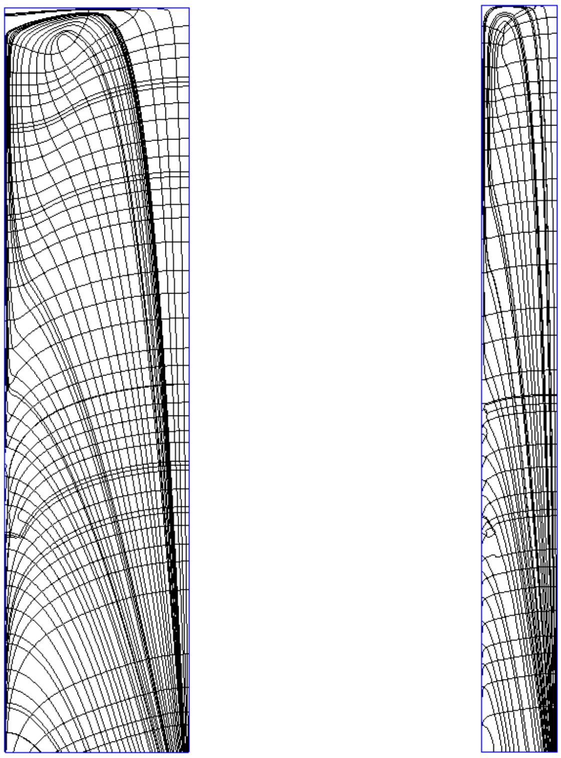

(a) (b)

Figure 12. NOSA-ITACA: distribution of the isostatic lines at collapse obtained for (a) [10 × 40] and (b) [4 × 40] cantilever masonry beams.

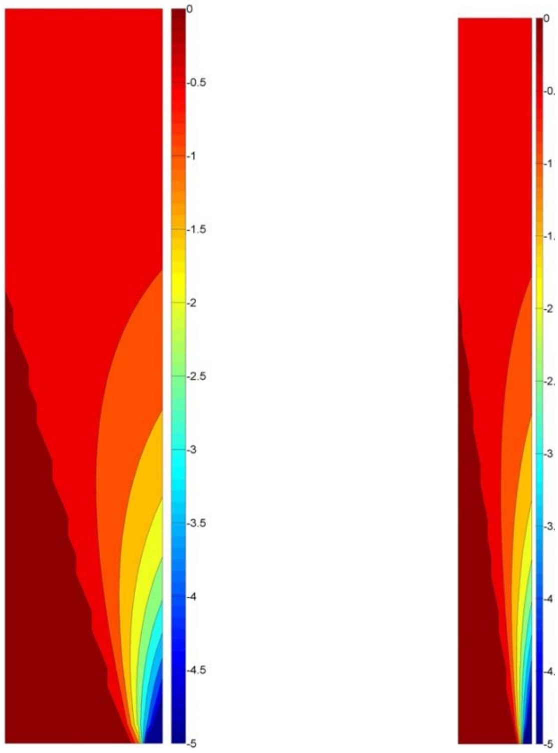

(a) (b)

Figure 13. MADY: distribution of the axial stress σ_z (MPa) at collapse for (a) [10 × 40] and (b) [4 × 40] cantilever masonry beams.

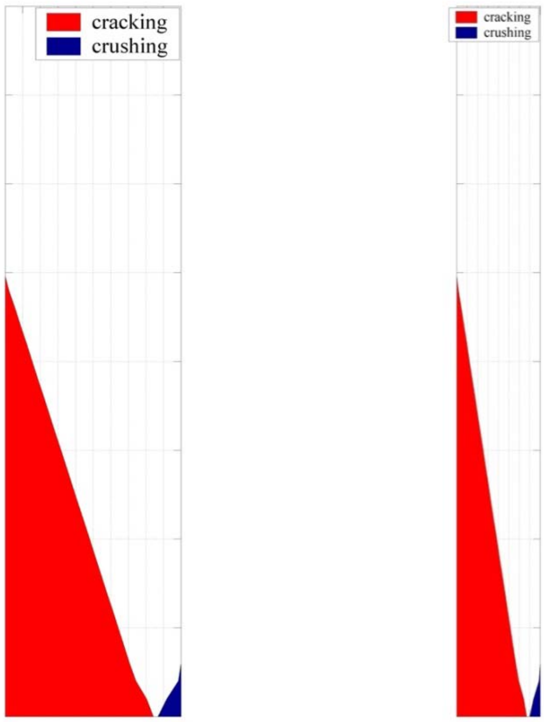

(a) (b)

Figure 14. MADY: distribution of the damage map at collapse for (a) [10 × 40] and (b) [4 × 40] cantilever masonry beams.

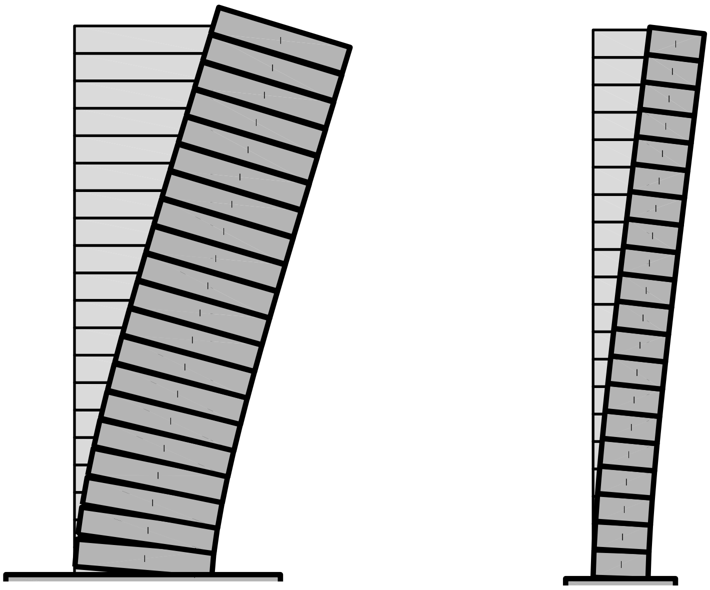

(a) (b)

Figure 15. SMARTmasonry: deformed shape at collapse for (a) [10 × 40] (displacement amplification factor 47.0) and (b) [4 × 40] (displacement amplification factor 7.5) cantilever masonry beams.

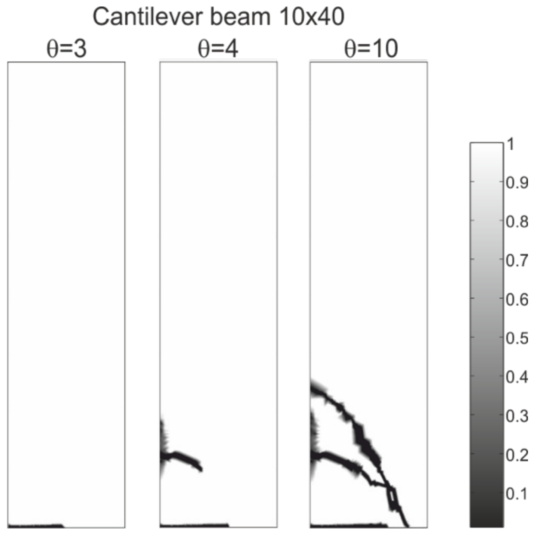

Figure 16. VDM: damage field *s* at different values of the drift θ for the [10 × 40] cantilever masonry beam.

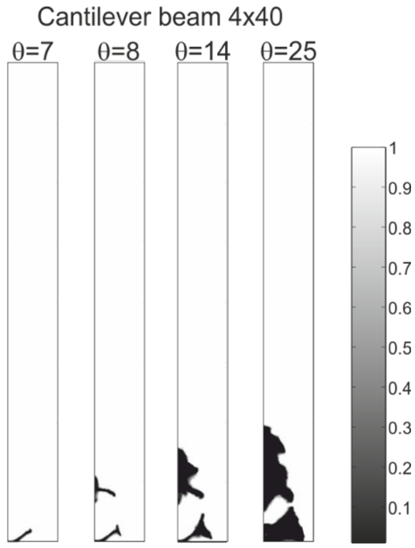

Figure 17. VDM: damage field s at different values of the drift θ for the [4 × 40] cantilever masonry beam.

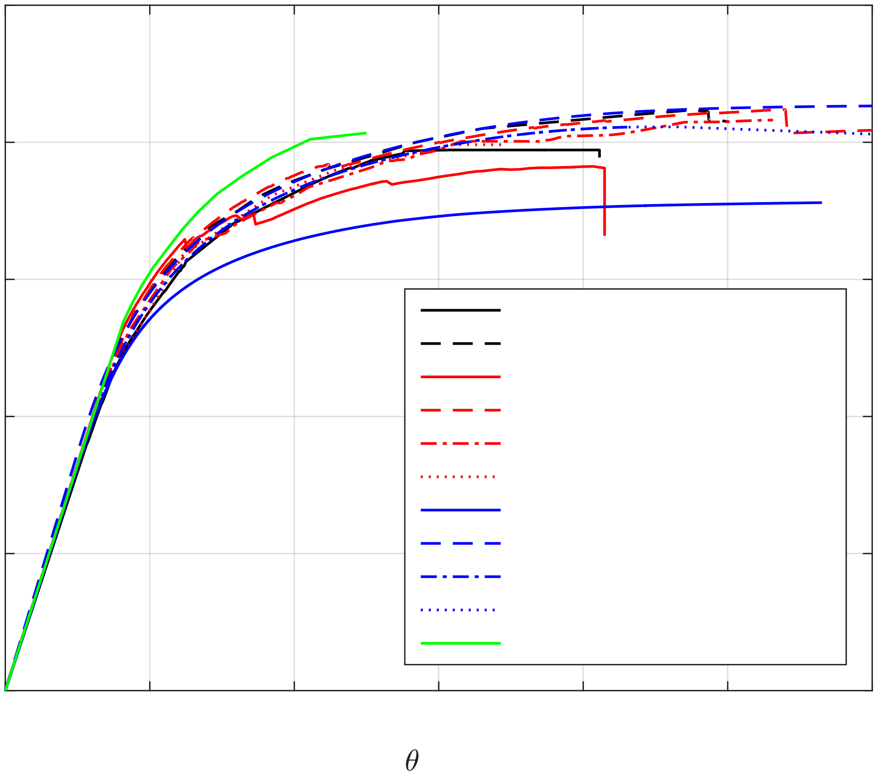

Figure 18. Comparison of pushover curves for [10 × 40] cantilever beam.

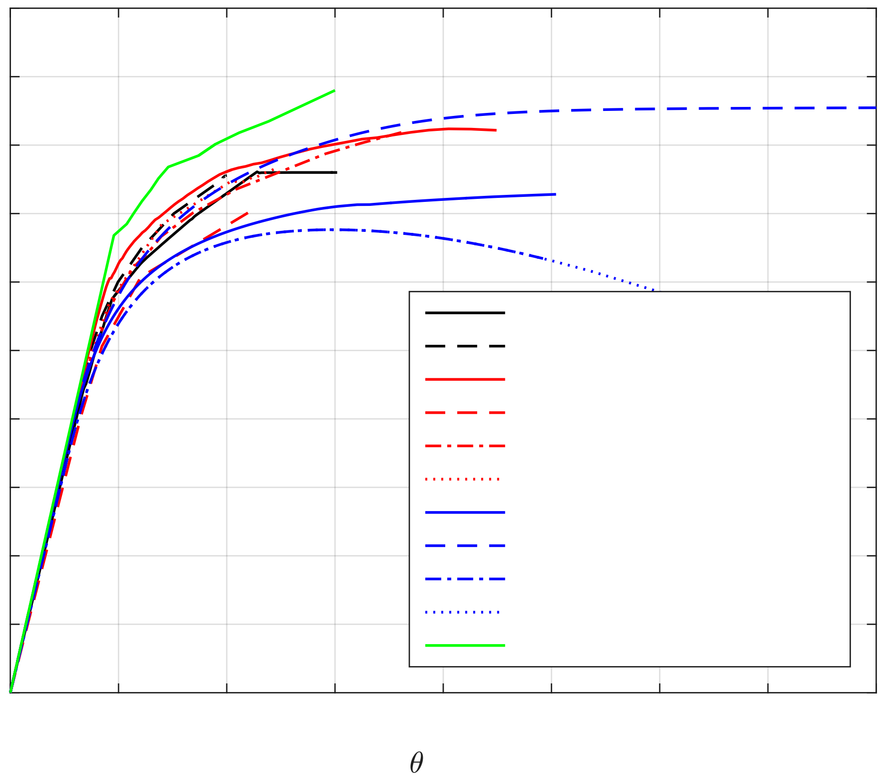

Figure 19. Comparison of pushover curves for [4 × 40] cantilever beam.

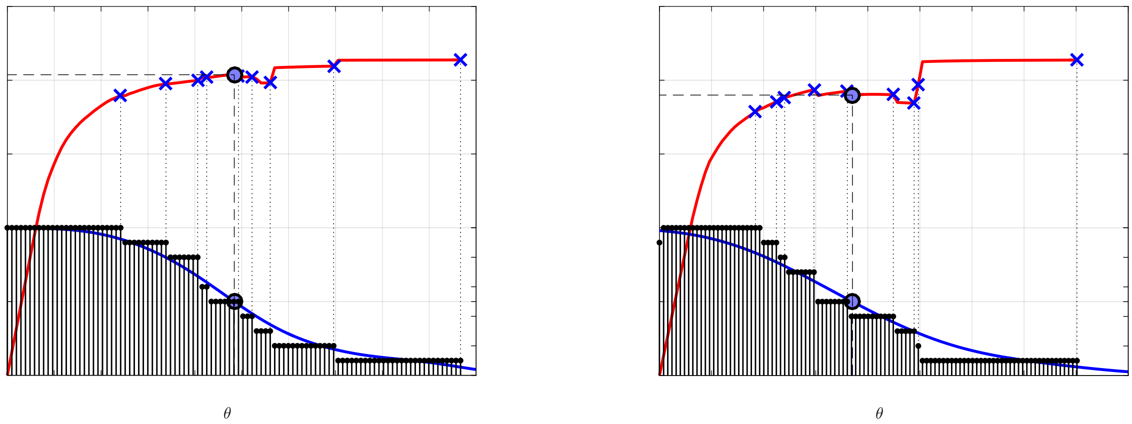

(a) (b)

Figure 20. Mean capacity curve for (a) [10 × 40] and (b) [4 × 40] beams. Collapse points for the various approaches are reported as crosses onto the curve, median value of the collapse displacement is reported as a heavy circle. The histogram below reports, at each displacement level, the number of analyses still active together with its curve fitting.

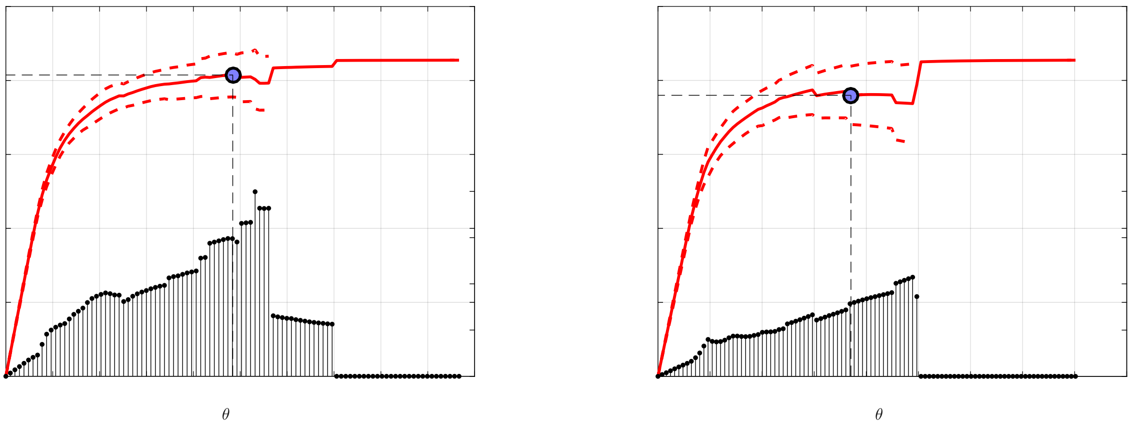

(a) (b)

Figure 21. Mean capacity curves (μ_i) for (a) [10 × 40] and (b) [4 × 40] beams. Median collapse point is reported as a solid circle onto the curve, dashed curves represent the curves $\mu_i+\sigma_i$ and $\mu_i - \sigma_i$. The histogram below reports, at each displacement level, the standard deviation of the value according to the curves, referring to still active analyses.

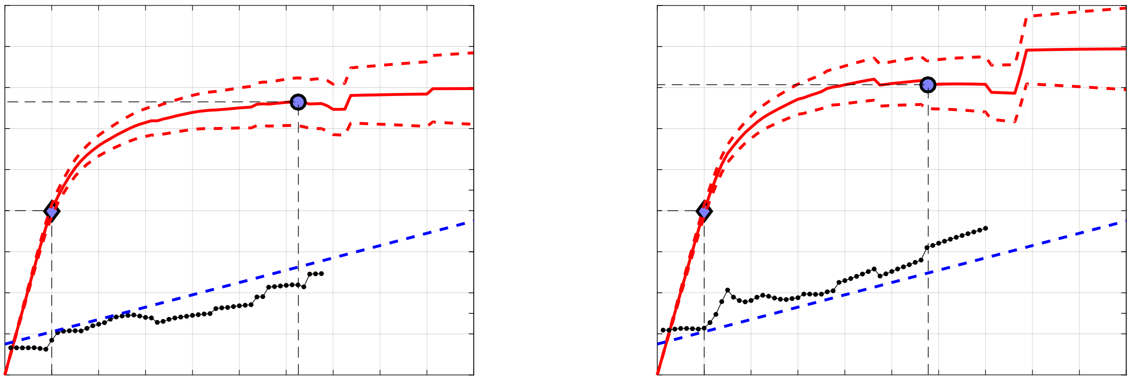

(a) (b)

Figure 22. Normalized mean capacity curves (μ_i) for (a) [10 × 40] and (b) [4 × 40] beams. Median elastic-limit and collapse points are reported as solid rhombus and circle onto the curve, red dashed curves represent the normalized curves $\mu_i+\sigma_i$ and $\mu_i - \sigma_i$. The graph below reports the CoV for the nondimensional curve (blue dashed line is the approximation reported in the text).